

**Report 2003.089**

**Interpretation of potential field data  
along the Lofoten continental margin  
Part I**

Report no.: 2003.089		ISSN 0800-3416	Grading: Confidential to 12.12.2008	
Title: Interpretation of potential field data along the Lofoten continental margin, Part I				
Authors: Odleiv Olesen, Jörg Ebbing, Jan Reidar Skilbrei & Erik Lundin			Clients: BP Norge, Norsk Hydro, Statoil, Oljedirektoratet and NGU	
County: Nordland and Troms			Commune:	
Map-sheet name (M=1:250.000) Mo I Rana, Bodø, Svolvær, Narvik and Andøya			Number of pages: 68	Price (NOK):
Fieldwork carried out: May-July, 2003			Date of report: 12.12.2003	Project no.: 3025.00
Person responsible:				
<p>Summary:</p> <p>Aeromagnetic data from the Røst Basin (RAS-03) were acquired in 2003 and compiled with neighbouring data-sets. The new Ra 3 compilation (Røst Aeromagnetics 2003 consisting of LAS-89, NAS-94, VAS-98 and RAS-3) has been reprocessed and subsequently merged with the SPT-93, NGU-69, NGU-73 and NRL-73 surveys in addition to the mainland of Norway aeromagnetic grid data. A compilation of the existing gravity data in the area has also been carried out. Forward 3D modelling along 14 profiles is constrained by available data on density, magnetic properties and reflection and refraction (OBS) seismics. The new data show that the previously interpreted oceanic fracture zones (Bivrost, Jenegga and Vesterålen) do not exist. Apparent offsets in the oceanic spreading anomalies were caused by poor navigation and wide line spacing of the vintage datasets. Consequently, opening of the Norwegian-Greenland Sea occurred along a stable axis without offsets of the oceanic spreading anomalies. A basement structure map has been compiled, and contains depth to magnetic basement, regional basement faults, and transfer zones. The Sandflesa and Flakstad basement highs at depths of approximately 6 km occur to the southwest and west of the Utrøst Ridge. The Bivrost, Vesterålen and Lenvik transfer zones define the regional segmentation of the Lofoten margin. The local Mosken and Melbu transfer zones are also located where shifts in polarity occur along faults and separate individual rotated fault blocks. The transfer zones are not spatially connected to younger oceanic fracture zones as previously interpreted. Depths to magnetic basement are locally larger than the depths obtained from gravity and seismic data (e.g. in the Helgeland and Vestfjorden basins and the Nordland Ridge). We interpret these to represent down-faulted Caledonian nappes, Devonian sediments or low-magnetic (amphibolite facies) Precambrian rocks. Voluminous mafic intrusions occur in both the basement and the overlying sediments in the Sandflesa high area and cause large gravity and magnetic anomalies. Basement depth estimates from gravity and magnetic data to the east of the Utrøst Ridge and north of the Marmæle Spur show that there may exist an approximately 2 km thick sequence of low-density sediments below the base-Cretaceous unconformity in this area.</p>				
Keywords: Geofysikk		Kontinentalsokkel		Tolkning
Berggrunnsgeologi		Magnetometri		Forkastning
Petrofysikk		Gravimetri		Fagrapport

## CONTENTS

1 INTRODUCTION.....	4
2 DATA SETS.....	5
2.1 Aeromagnetic data.....	5
2.2 Gravity data.....	7
2.3 Petrophysical data.....	9
2.4 Bathymetric and topographic data .....	12
2.5 Seismic studies.....	13
3 INTERPRETATION METHODS.....	13
3.1 Data presentation and geophysical interpretation map .....	13
3.2 Interpretation of depth to anomaly sources .....	14
3.3 3D modelling .....	17
4 STRUCTURAL FRAMEWORK.....	25
5 RESULTS .....	30
5.1 3D gravity model.....	30
5.2 3D magnetic structure .....	32
5.3 Oceanic magnetic anomalies .....	41
5.4 Regional structures .....	43
6 CONCLUSIONS.....	55
7 RECOMMENDATIONS FOR FURTHER WORK.....	57
8 ACKNOWLEDGEMENTS.....	57
9 REFERENCES.....	58
List of figures, tables and maps.....	65

## 1 INTRODUCTION

The present study is part of the Røst Aeromagnetics 2003 Project (Ra 3) financed by BP Norge, Norsk Hydro, Statoil, the Norwegian Petroleum Directorate and the Geological Survey of Norway. BP Norge joined the project as a late participant in July 2003. The survey area extends from 66° to 69°45'N and from 6°45'E to the Swedish border. The focus area is the Utgard High - Sandflesa High - Utrøst Ridge - Røst Basin area. New aeromagnetic data (RAS-03) were acquired in the Røst Basin, an area that remains unexplored for petroleum. The objective of Ra 3 Project is to improve our understanding of the tectono-magmatic setting along the Lofoten continental margin. Various and partly contradicting interpretations of the regional structural elements have been put forward during the last years. We have updated and reprocessed the aeromagnetic and gravity databases from the area to help resolve some of these inconsistencies. The data compilations provide most new information in the western part of the Nordland area, i.e. in the Røst Basin – Utrøst Ridge – Utgard High area.

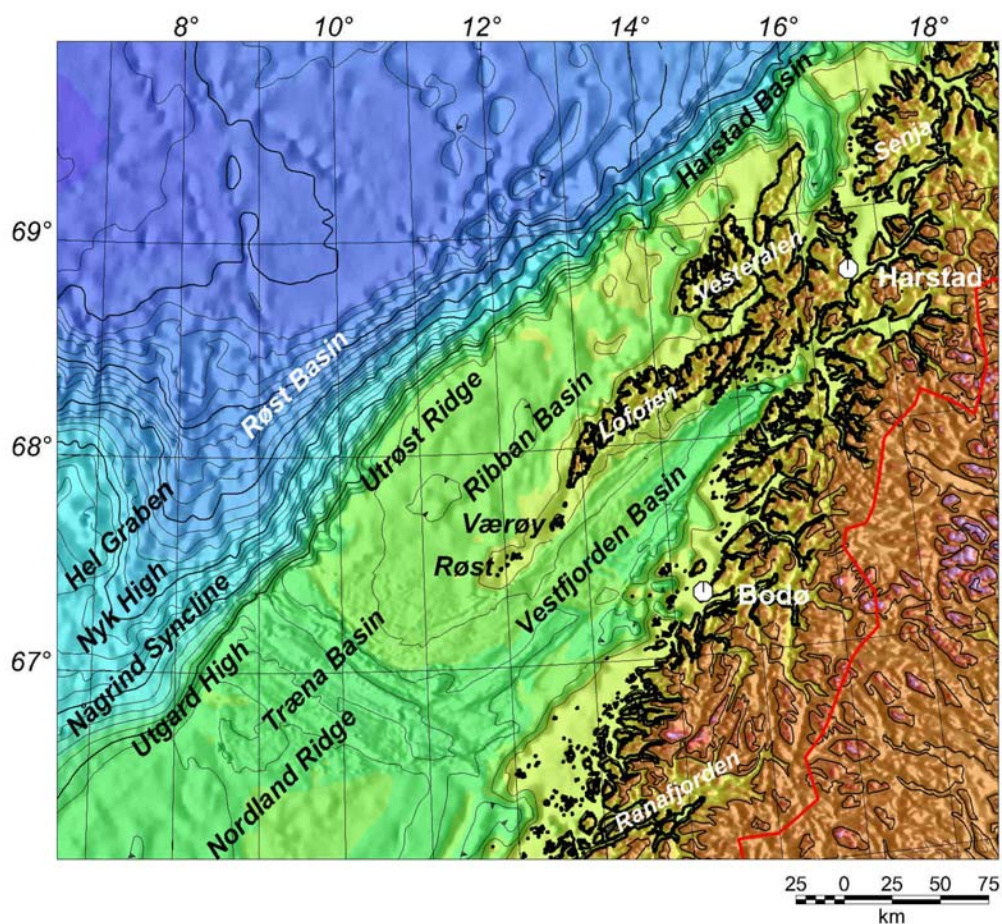


Figure 1.1 Bathymetry and topography, Nordland area, 100 and 500 m contour intervals.

## 2 DATA SETS

### 2.1 Aeromagnetic data

A total of eight offshore aeromagnetic surveys (Fig. 2.1) have been compiled in the present project. Specifications for these surveys are shown in Table 2.1. Vintage data that were reflight in 1989, 1994, 1998 and 2003 are not included in the table, and are also excluded in the final map compilation. The pattern of flight lines generally provides data along NW-trending profiles with a spacing of 2-5 km. The LAS-89 (Olesen & Myklebust 1989), NAS-94 (Olesen & Smethurst 1995), VAS-98 (Mauring et al. 1999) and RAS-03 (Mauring et al. 2003) surveys have been processed within the Ra-3 project using the loop closure method (Mauring et al. 2003). This new data compilation has been merged with the SPT-93, NGU-69, NGU-73, NRL-73 and the mainland of Norway grid using the minimum curvature GRIDKNIT software from Geosoft (2000a). The NGU-69 and NGU-73 surveys were reprocessed separately using the median levelling technique (Mauring et al. 2002) before the merging of the grids. We have used the Verhoef et al. (1996) version of the NRL-73 dataset (Vogt et al. 1981) to the northwest of the NGU-73 survey. The NRL-73 dataset includes some ship-lines in the western part of our project area. The mainland of Norway grid has been digitised into a 500x500 m matrix from manually drawn contour maps. The Definite Geomagnetic Reference Field (DGRF) has been subtracted (Nor. geol. unders. 1992). The area was flown at different flight altitudes and line spacing dependent on the topography.

*Table 2.1. Offshore aeromagnetic surveys compiled for the present study (Figs. 3.1 & 3.2, Maps 1 & 2). We included 27.000 km of the NAS-94 survey. The RAS-03 survey included 2.300 km reflight of the LAS-89 survey.*

Year	Area	Operator	Survey name	Navigation	Sensor elevation m	Line spacing km	Length km
1969	69° - 70°N	NGU	NGU-69	Decca	200	4	500
1973	Vøring Basin Marginal High	NGU	NGU-73	Loran C	500	5	2.500
1973	Norwegian Sea	Naval Research Lab.	NRL-73		300	10-20	1.500
1989	Lofoten	NGU	LAS-89	GPS/ Loran C/ Syledis	250	2	30.000
1993	Hel Graben- Nyk High	World Geo-science	SPT-93	GPS	80	0.75	19.000
1994	Nordland Ridge- Helgeland Basin	NGU	NAS-94	GPS	150	2	27.000 (36.000)
1998	Vestfjorden	NGU	VAS-98	GPS	150	2	6.000
2003	Røst Basin	NGU	RAS-03	GPS	230	2	30.000

Table 2.2. On land aeromagnetic surveys compiled for the present interpretation project (Figs. 3.1 - 3.2, Maps 1 - 2).

Year	Area	Operator	Navigation	Sensor elevation	Line spacing km	Recording
1964	Andøya	NGU	Visual	150 m above ground	1	Analogue
1965	Vesterålen area	NGU	Visual	300 m above ground	2	"
1971-73	Nordland-Troms	NGU	Decca	1000 m above sea level	2	"

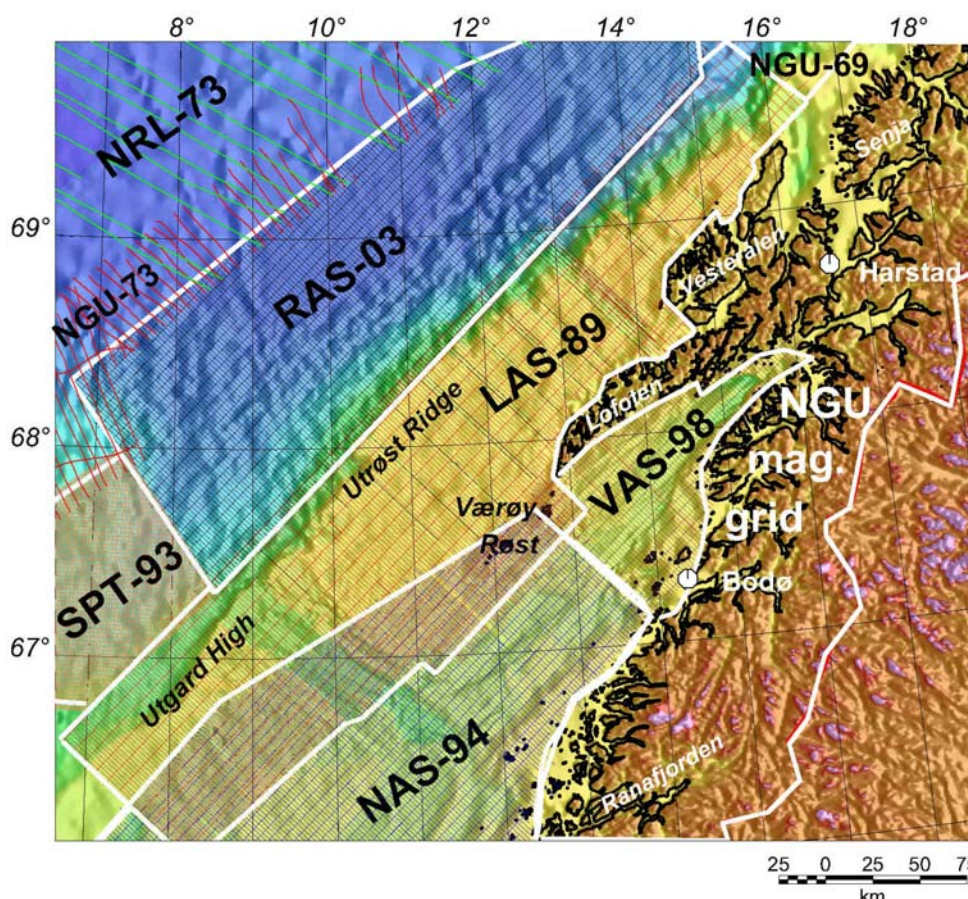


Figure 2.1 Compilation of aeromagnetic surveys in the Nordland area. NRL-73 US Naval Research Laboratory 1973, RAS-03 - Røst Aeromagnetic Survey 2003, SPT-93 - Simon Petroleum Technology 1993, LAS-89 - Lofoten Aeromagnetic Survey 1989, NAS-94 - Nordland Aeromagnetic Survey 1994, VAS-1998 - Vestfjorden Aeromagnetic Survey 1998. The latter four surveys were acquired by the Geological Survey of Norway.

Specifications for the different sub-areas are given in Table 2.1. The grids were trimmed to c. 10 km overlap and merged using a minimum curvature algorithm, GRIDKNIT, developed by Geosoft (2000a). The final grid shown in Fig. 3.1 was displayed using the shaded-relief technique with illumination from the southeast. To enhance the high frequency component of the Ra 3 dataset a 25 km Gaussian high pass filtered map of the compiled data-set has been produced (Fig. 3.2). The location of flow basalts and sills are more visible on this map than on the total field map. A grey tone shaded relief version of a 10 km high-pass filtered grid is superimposed on both the coloured total field map and the 25 km high-pass filtered map (Figs. 3.1 & 3.2 and Maps 1 & 2). The contour intervals of the aeromagnetic maps in Figs. 3.1-3.2 and Maps 1-2 are 20 nT (thin lines) and 100 nT (bold lines).

## 2.2 Gravity data

The marine gravity data consisting of 37.000 km of profiles collected by the Norwegian Petroleum Directorate, the Norwegian Mapping Authorities and various geophysical companies have been levelled using the median levelling technique (Mauring et al. 2002). The present study is in addition based on measurements from 6100 gravity stations on land (Table 2.3 & Fig. 2.2). The compiled free-air dataset has been interpolated to a square grid of 2 km x 2 km using the minimum curvature method (Geosoft 2001). The simple Bouguer correction at sea (Mathisen 1976) was carried out using a density of 2200 kg/m<sup>3</sup>. The International Standardization Net 1971 (I.G.S.N. 71) and the Gravity Formula 1980 for normal gravity have been used to level the surveys. The compiled grid was merged with gravity data from satellite altimetry in the deep-water areas of the Norwegian Sea (Andersen & Knudsen 1998). The location of the marine profiles are shown in Fig. 2.2 while Fig. 3.3 and Map 3 show the free-air gravity field of the Nordland area. Fig. 3.4 and Map 4 show the Bouguer gravity data.

An Airy-Heiskanen 'root' (Heiskanen & Moritz 1967) was calculated from a compiled topographic and bathymetric data-set (see Fig. 1.1 and section 2.4 below). The gravitational attraction from the 'root' was calculated using the AIRYROOT algorithm (Simpson *et al.* 1983). The isostatic residual (Fig. 3.5, Map 5) was achieved by subtracting the gravity response of the Airy-Heiskanen 'root' from the observed Bouguer gravity data. A 100 km Gaussian high pass filtered map of the compiled Bouguer gravity data-set has also been produced (Fig. 3.6 and Map 6). The contour intervals of the gravity maps in Figs. 3.3-3.6 and Maps 3-6 are 2 mGal (thin lines) and 10 mGal (bold lines).

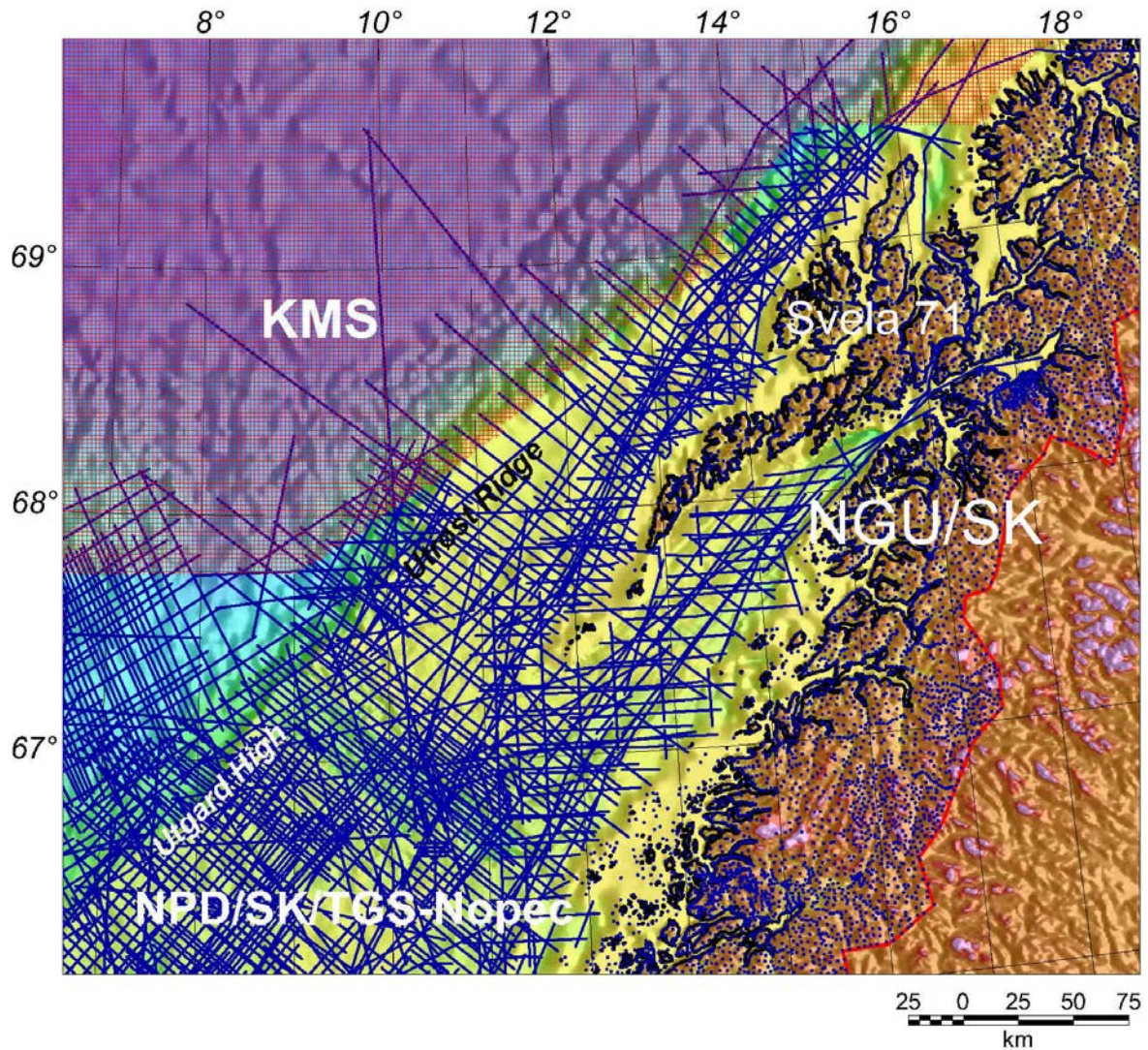


Figure 2.2 Compilation of gravity surveys in the Nordland area. KMS – Kort og Matrikelstyrelsen, Denmark, NPD/SK- Norwegian Petroleum Directorate/ Norwegian Mapping Authority.

Table 2.3. Gravity surveys on land (Skilbrei et al. 2000) included in the present study (Fig. 2.2, Figs. 3.3-3.6, Map 3 - 6).

Survey stations	Area	No. of stations
Geological Survey of Norway	Nordland and Troms	8268
Norwegian Mapping Authority	Nordland and Troms	953
Svela (1971)	Lofoten - Vesterålen	306
<b>Total</b>		<b>9527</b>



## 2.3 Petrophysical data

The pronounced magnetic and gravimetric anomalies within the project are continuous from land onto the continental shelf (Figs. 3.1 - 3.6). It is important to know the density and magnetic properties of the rocks on land when interpreting the potential field data in the offshore area. Approximately 4700 rock samples (Table 2.4, Fig. 2.3), collected during geological mapping and geophysical studies have been measured with respect to density, susceptibility and remanence (Olesen *et al.* 1997b, 2002).

The high-amplitude magnetic anomalies in the Lofoten-Vesterålen and northwestern part of Senja are caused by granulite-facies gneisses and intrusives (mangerites). The Q-values are generally low, in the order of 0.5 or lower. Especially mafic and ultramafic rocks show, however, frequently high Q-values. These rocks give arithmetic means as high as 0.9 in the Lofoten area while the logarithmic mean is 0.3. Schlinger (1985) and Olesen *et al.* (1991) have also shown that the remanence of the rocks in the Lofoten-Vesterålen area is viscous and parallel to the present Earth's field, which simplifies the aeromagnetic interpretations in the area.

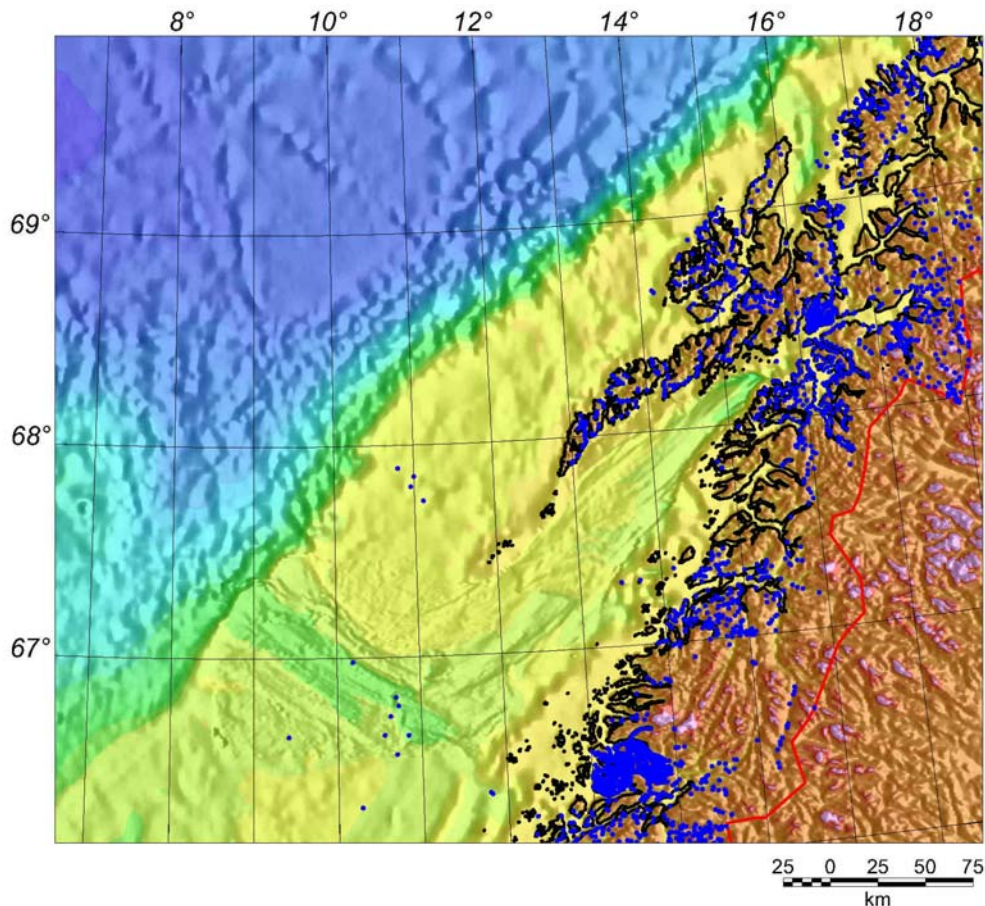


Figure 2.3 Locations of petrophysical samples on the mainland and offshore Nordland shown as blue circles (Olesen *et al.* 1997b, 2002, Mørk & Olesen 1995, Mørk *et al.* 2002).

The orthopyroxene isograd in the Vesterålen area coincides with the boundary between the high-magnetic and low-magnetic gneisses. The migmatites to the west of this line are in granulite-facies metamorphism whereas to the east they have amphibolitic metamorphic grade. In this particular area

the magnetic basement surface reflects the depth to the granulite-facies gneisses. The medium amplitude magnetic anomalies on the mainland are mostly caused by granitic and quartz-dioritic rocks and migmatitic gneisses. The average density for all basement rocks in the Lofoten-Vesterålen area is 2780 kg/m<sup>3</sup> (Table 2.4) The average density for the Middle, Upper and Uppermost Allochthons, which constitute the bulk of the Caledonides within the Nordland area, is 2810 kg/m<sup>3</sup>. The susceptibility of the Caledonian rocks is mostly low, with exceptions of some banded iron formations and mafic intrusions that frequently show high values. These units appear as high-frequency magnetic anomalies on the mainland (Figs 3.1 & 3.2 and Maps 1 & 2). The magnetically transparent Caledonian nappes in southern Nordland extend to the northwest below the Helgeland Basin and the Nordland Ridge causing the large depth to magnetic sources in this area (Figs. 3.2 & 3.2 and Maps 1 & 2).

We have applied information from petroleum exploration wells as constraints for the potential field modelling. Densities of sedimentary sequences calculated from well logs, refraction seismic profiles and previous interpretation reports in the Nordland area are shown in Table 2.5. Numbers in parentheses show depth of base of the different sequences. Magnetic properties of Tertiary igneous rocks from the Vøring area are shown in Table 2.6.

*Table 2.4 Arithmetical mean and standard deviation of density, susceptibility and Q-values measured on 4700 hand specimens from the Nordland area. The measurements were extracted from the national petrophysical database at the Geological Survey of Norway. Olesen et al. (1991), Mørk & Olesen (1995) and Olesen et al. (1997b,2002) have reported more detailed presentations of the statistical data. SI units are used.*

Rock Unit/Type	No.	Density		Q-value		Susceptibility	
		mean	std.	mean	std.	mean	std.
Uppermost Allochthon							
Rödingsfjell Nappe Complex	821	2787	137	3.26	12.8	0.0060	0.034
Helgeland Nappe Complex	488	2811	126	4.41	15.9	0.0032	0.018
Bindal Batholith	304	2738	136	3.30	11.6	0.0040	0.014
Upper Allochthon							
Narvik Nappe Complex	164	2811	130	1.60	4.6	0.0032	0.017
Precambrian Basement							
Senja, Kvaløy and Ringvassøy, gneiss etc.	384	2716	106	2.11	5.4	0.0078	0.020
Senja, Kvaløy and Ringvassøy, greenstone belts	125	2942	136	0.46	0.6	0.0266	0.059
The Lofoten area	470	2764	130	1.36	5.6	0.0339	0.050
Tysfjord Granite Complex	607	2678	79	1.22	4.0	0.0074	0.024
Sjona-Høgtuva tectonic windows	1140	2643	39			0.0084	0.012

Table 2.5 Density (in 1000\*kg/m<sup>3</sup>) of sedimentary sequences from density logs of wells in the Nordland area and refraction seismic studies. (2.78\*) = average density of 639 rock samples from the Precambrian on the Lofoten and Vesterålen archipelago (Olesen et al. 1997b, 2002).

	Well 6609/7-1 Phillips Petroleum  Nordland Ridge	Wells 6607/5-1 and -2 Esso  Utgard High	Well 6507/2-1 Norsk Hydro  Dønna Terrace	IKU wells 6611/09-U-01 and -02 Helgeland/ Brønnøysund Basin	Density estimates from sonobouys Univ. of Bergen	Density estimates from refraction seismics Mjelde et al. (1998) Sandflesa area	Density adapted for modelling
Water depth	250m	368m	381m	352-355 m			1.03
Start of log	1025m	900m	1050m				
Pleistocene		2.21 (1220m)					
Plio- Pleistocene						2.00	2.03
Tertiary	2.10 (1635m)	2.21 (2510m)	2.18 (2005m)		2.25	2.15	2.23
Upper Cretaceous						2.20	
Lower Cretaceous						2.45	
Cretaceous	2.25 (1845m)	2.32 (3785m+)	2.37 (3610m)		2.30		2.35
Jurassic			2.54 (4400m+)		2.35	2.60	2.50
Triassic				2.58 (280m+)		2.60	2.60
Permian	2.31 (1920m)			2.58 (560m+)			
Caledonian nappes							2.81
Basement	2.64 (1960m+)				2.70-2.85	2.70-2.80	2.75-2.85 (2.78*)
Lower crust						3.10-3.23	2.95-3.00
Sill		2.92 (3792- 3886m)					2.95
Sill		2.98 (4640- 4697m)					
Magmatic underplating							3.10
Mantle							3.30

*Table 2.6. Magnetic properties of igneous rocks from drilling in the Vøring area within the Deep Sea Drilling Project (DSDP) and Ocean Drilling Program (ODP) in 1974 and 1985, respectively (<sup>1</sup>Kent & Opdyke 1978, <sup>2</sup>Eldholm et al. 1987). The ODP susceptibility data are claimed to be cgs-units, but they are most likely in SI-units, because a corresponding magnetite content of 30-40 % in the volcanics is highly unlikely. A log diagram of the 642E well in Schönharting & Abrahamsen (1989) supports this conclusion.*

Site	Penetration	Number of samples	NRM (A/m)	Suscept. (SI)	Polarity	Mean inclination
338 <sup>1</sup>	437 m	7	3.1	0.016	Normal	70.4°
342 <sup>1</sup>	170 m	3	1.4	0.015	Reversed	-81.0°
642E <sup>2</sup>	1229 m	221	5.0	0.030	Reversed	-63°

## 2.4 Bathymetric and topographic data

The bathymetry data for the deep-water part of the map (Fig. 1.1) come from satellite altimeter data released by Smith and Sandwell (1997). The bathymetric data from the shallow water areas were compiled by The Norwegian Mapping Authority, Marine Department in Stavanger. This data set has three different sources; 1) modern multi-beam echo sounder in the Vestfjorden area, 2) digitised naval maps in areas adjacent to the coast and 3) depth data collected during seismic surveys in areas further offshore. The quality of these data varies considerably. Data set 1 has the highest quality while data set 3 is poorest. The cell size of the combined grid is 1 km x 1 km.

Very coarse data to fill in the gaps in coverage were extracted from a global data set supplied with the ER-Mapper software. High-resolution topography data (100m x 100m) for Norway were supplied by the Norwegian Mapping Authority. Topography for Sweden was downloaded from the GTOPO30 data set

(<http://edcwww.cr.usgs.gov/landdaac/gtopo30/gtopo30.html>). The final grid shown in Fig. 1.1 was displayed using the shaded-relief technique with illumination from the southeast. The grey tone part of the maps is calculated from a 20 km high pass filtered grid and is superimposed on the coloured elevation model.

## **2.5 Seismic studies**

In the area interpretations of Ocean Bottom Seismograph (OBS) arrays are available from the studies of Mjelde et al. (1992, 1993, 1997, 1998). The results of the OBS arrays have been interpreted along profiles, providing a good coverage of the study area.

Further structural interpretations are available by Blystad et al. (1995). Brekke & Riis (1987), Brekke (2000), Eldholm et al. (2002), Berndt et al. (2000, 2002), Lundin & Doré (1997), Løseth & Tveten (1996), Skogseid et al. (1992) and Tsikalas et al. (2001, 2002) present additional interpretations from reflection seismic profiles along the margin. The information of these studies was considered, wherever possible, to constrain the modelling and analysis results.

## **3 INTERPRETATION METHODS**

### **3.1 Data presentation and geophysical interpretation map**

Histogram-equalised colour (i.e. each colour cover the same area on the map), high-frequency filtered and shaded-relief images have been used to enhance the information of the regional data-sets. Shaded-relief presentations, which treat the grid as topography illuminated from a particular direction, have the property of enhancing features that do not trend parallel to the direction of illumination. The aeromagnetic and gravity maps (Maps 1 - 6) are produced at a scale of 1:500.000. These maps are also presented in A3 format in Figs. 3.1 – 3.6. The separation of the residual field on the magnetic and gravity datasets is carried out in the frequency domain using 25 and 100 km Gaussian filters, respectively. A shaded relief version in black/white of the 10 km high pass filtered aeromagnetic grid is superimposed on both the coloured total field and 25 km high-pass filtered aeromagnetic grid (Figs. 3.1 & 3.2 and Maps 1 & 2).

The grid data-sets were analysed with the Oasis Montaj software (Geosoft 2000b, 2001). Fault zones within the basement and partly within the sediments are interpreted from the aeromagnetic map. The fault zones are characterized by (Henkel & Guzmán 1977, Henkel 1991):

1. Linear discordances in the anomaly pattern.
2. Displacement of reference structures.
3. Linear gradients.
4. Discordant linear magnetic minima (only visible over shallow magnetic basement).

The faults are plotted on Figs. 3.1 - 3.7, 5.14, 5.15 and Maps 1 - 7. High frequency anomalies

representing volcanic rocks are also included. These anomalies are often negative. The interpreted location of the easternmost boundary of the flow basalts (Blystad et al. 1995, Tormod Henningsen pers. comm. 2003) in the Røst Basin is added to the geophysical maps in addition to the lava windows proposed by Tsikalas et al. (2001). The combined interpretation of depth estimates from both gravity and aeromagnetic data (see section 3.2 below) has been carried out by interpolation and contouring of depth to basement (Figs. 3.7, 5.15, and Map 7). In areas where the two datasets give diverging depth estimates (e.g. the Helgeland and Vestfjorden basins and the Nordland Ridge) the gravity interpretation is given the highest weight, especially in areas where we expect to find low-magnetic basement continuing from onshore or down-faulted, amphibolite facies gneisses or Caledonian nappes within the deep basins. High frequency anomalies interpreted to represent magnetic volcanics are excluded in the contouring. All individual depth estimates from the gravity and aeromagnetic interpretation are plotted on the maps (Figs. 3.1 - 3.7 and Maps 1 - 7).

### **3.2 Interpretation of depth to anomaly sources**

Depths to basement have been estimated from inversion of aeromagnetic and gravity data, applying the autocorrelation algorithm of Phillips (1979), the 3D Euler deconvolution algorithm of Reid *et al.* (1990) and a least-squares optimising algorithm of Murthy & Rao (1989). We have utilised the software versions implemented by Torsvik & Olesen (1992), Geosoft (2003) and Torsvik & Fichler (1993), respectively. In addition, we applied the 'AutoMag software' (Encom 2003) that utilises the profile method of Naudy (1971) and provides the interpreter with the ability to quickly test any solution against forward model solutions. The Euler 3-D deconvolution method (Reid et al., 1990; Geosoft 2003) was used to estimate the depth to magnetic rocks within both the crystalline basement and the Palaeozoic intra-sedimentary volcanics. The depths to the magnetic sources constrain the interpretation of the basement anomalies and aid in the separation of anomalies related to basement structures from anomalies related to younger intrusives.

The autocorrelation method is assuming that the magnetic basement is defined as a two-dimensional (2D) surface constructed from a large number of thin vertical 'dykes' of differing magnetisation. The upper terminations of the 'dykes' define the basement surface. The depth to this surface is estimated by passing a short window along the magnetic profile, estimating a depth for each position of the window. A total of 611 autocorrelation depth estimates are plotted on Figs. 3.1 - 3.7 and Maps 1 - 7. The method has the advantage that sources at different depths can be separated, i.e. anomalies caused by deep and shallow bodies in the same profile. This is

especially useful in the western Lofoten area where abundant lava flows/sills occur within the sedimentary sequence.

The Euler's homogeneity equation relates the potential field (either magnetic or gravity) and its orthogonal derivative components to the location of the source, given an assumed rate of change of the field with distance. This rate of change (degree of homogeneity) can be interpreted as a structural index describing the form of the source structure (Thompson 1982). The method has the advantages of being applicable to anomalies caused by a wide variety of geological structures and being independent of remanent magnetisation and ambient field direction.

The Euler 3-D deconvolution method requires gridded potential field data as input. We chose to compute Euler depth solutions for a 'thick step'-type source geometry where the interface between magnetic and non-magnetic rocks is step-shaped. This geometry is applicable to, for example, a faulted magnetic basement. We have also computed depths using 'contact'- and 'thin plate'-type models where magnetic and non-magnetic materials are juxtaposed on a continuous planar surface. In the western part of the study area, where the high- to intermediate- frequency anomalies are believed to be caused by intrasedimentary volcanic rocks, 'thin plate'-type models were applied (dykes, sill and flows). In the eastern and central part of the study area, the source position derived from the 'thick step' model were better focused in position and consistent with basement depths seen in seismic data. Reid et al. (1990) and numerous interpretation reports on the Mid Norwegian continental shelf (e.g. Olesen & Smethurst 1995; Skilbrei et al. 2002) conclude that structural indices between zero and unity are appropriate for basement anomalies similar in form to those of the present study. Experiences from the other studies on the Norwegian continental shelf show that flat-lying sills and basalt flows produce anomalies in the order of 2-3 nT (Olesen & Myklebust 1989, Skilbrei et al. 2002).

We applied the improved 'Located Euler 3D method' making use of the analytic signal to locate edges of the magnetic field sources. The Blakely & Simpson (1986) grid peak-picking algorithm locates the crest of the analytic signal anomalies improving the location of the depth estimates. The window size for this analysis is determined from the location of the adjacent anomaly inflection points. The Located Euler method produces fewer solutions than the Standard Euler method and the spray-pattern of source positions commonly observed in Euler depth solutions is avoided. The individual depth estimates are plotted as small circles with colour fills depending on depth (Fig. 3.1 – 3.7 and Maps 1 –7). The number of solutions is reduced using an iterative median filtering technique (Olesen & Smethurst 1995). The individual filtered depths are plotted on the maps as numbers and annotated with 'x' for structural index 1 and '+' for structural index 0.5.

In addition to the grid depth analysis, we analysed single profiles and complete anomalies from the areas of the Utgard High and the Nyk High, using the Naudy method (Naudy, 1971) which is implemented in the 'Automag' software (Encom 2003). The Automag software is used for automatic location and inversion of magnetic anomalies. The vertical gradient was calculated from the total field anomalies in order to sharpen the anomalies, and to reduce the anomaly overlap problems. The ideal window size was adjusted during the analysis to span both the minimum and maximum amplitude points of the anomaly. When profiles were not oriented perpendicular to the magnetic field contours, a strike correction to the bodies creating the anomalies has been applied. This is done to avoid overestimation of apparent depths because a profile crosses a feature obliquely. Finally, the depth results were compared with the located Euler deconvolution method. The located Euler solutions represent a semi-automated methodology. The selection and critical examination of results was done at the basement depth contouring level. The results from the Naudy method have been plotted on the geophysical maps together with the Euler depths and the results from the autocorrelation method.

The 2D magnetic depth estimates and gravity inversion profiles have been reported earlier by Olesen & Torsvik (1993). A combined depth-to-basement map has been constructed from the magnetic and gravity depth estimates. In areas where the gravity and magnetic datasets give diverging depth estimates the gravity interpretation is given highest priority, especially in areas where we expect to find shallow, low-magnetic basement continuing from onshore areas or as a result of down-faulted Caledonian nappes or amphibolite facies gneisses within the deep basins. High frequency anomalies interpreted to represent magnetic volcanics were excluded in the contouring.

Fault zones within the basement and partly within the volcanics were interpreted from the geophysical images. High gravity gradients along the basin boundaries are generally interpreted to be caused by faults but may in some cases be related to steeply dipping sedimentary bedding.



### **3.3 3D modelling**

The 3D forward modelling of the gravity and magnetic fields has been done with the modelling software IGMAS (Interactive Gravity and Magnetic Application Software: Götze & Lahmeyer 1988, Schmidt & Götze 1998, Breunig et al. 2000).

The model of the Nordland area is mainly based on the density model of Olesen et al. (2002) and references therein. Applied density estimates of sediments and basement are shown in Tables 2.6 while published magnetic properties of volcanic rocks in the Vøring area are displayed in Table 2.4 and 2.6. The Moho topography and lower crustal densities have been deduced from published OBS seismic data (Mjelde et al. 1992, 1993, 1997, 1998).

The model consists of 14 parallel cross-sections in the study area with a distance of 20-35 km (Figs. 5.4 – 5.13). In addition, the model was extended 5000 km in each direction to avoid edge effects. In the central part of the model the location of the cross sections coincides with the location of the OBS profiles presented by Mjelde et al. (1992). Ten of the model cross sections are presented in Figs. 5.4 – 5.13.

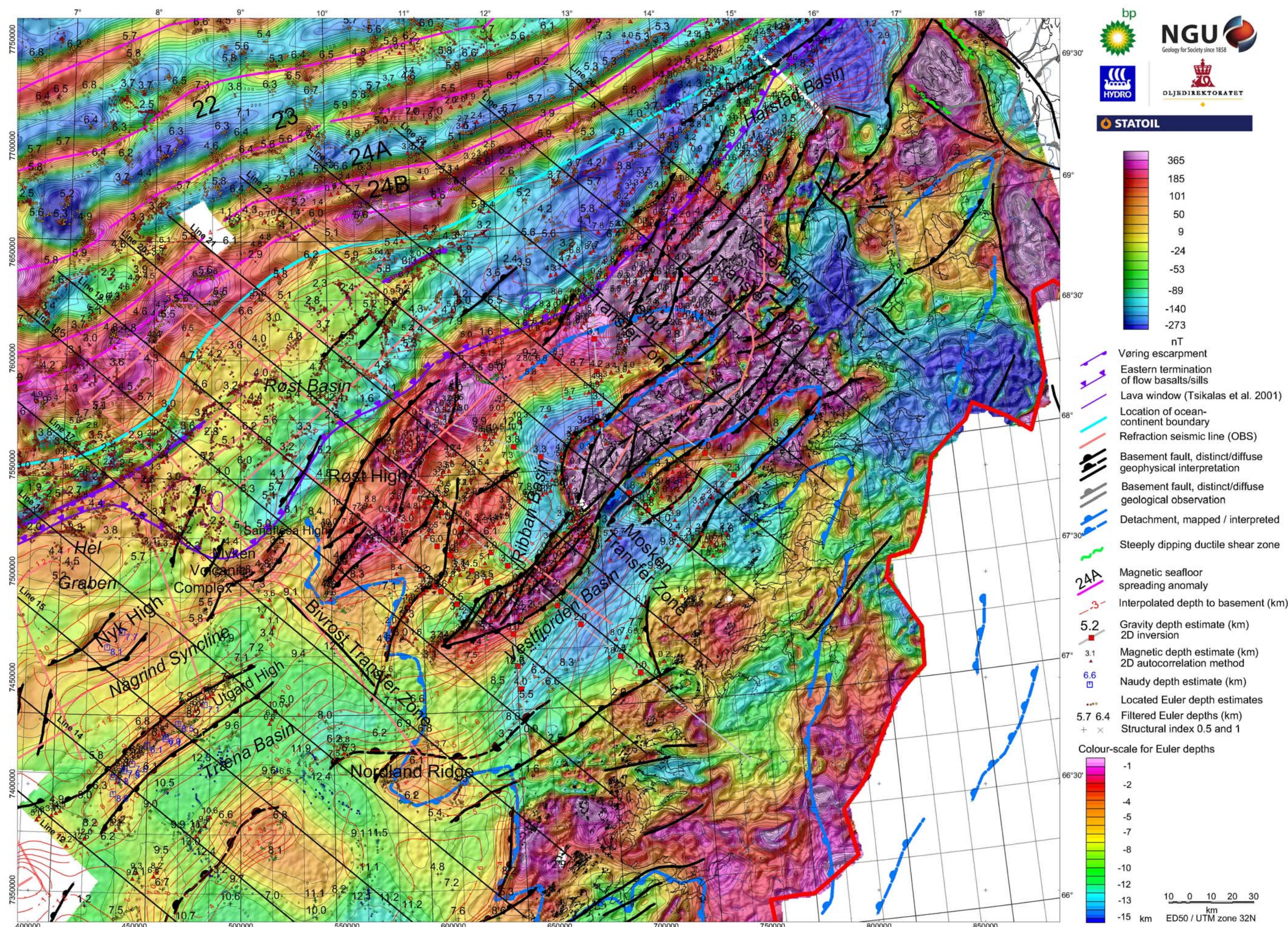


Figure 3.1 Aeromagnetic anomaly map, Nordland area

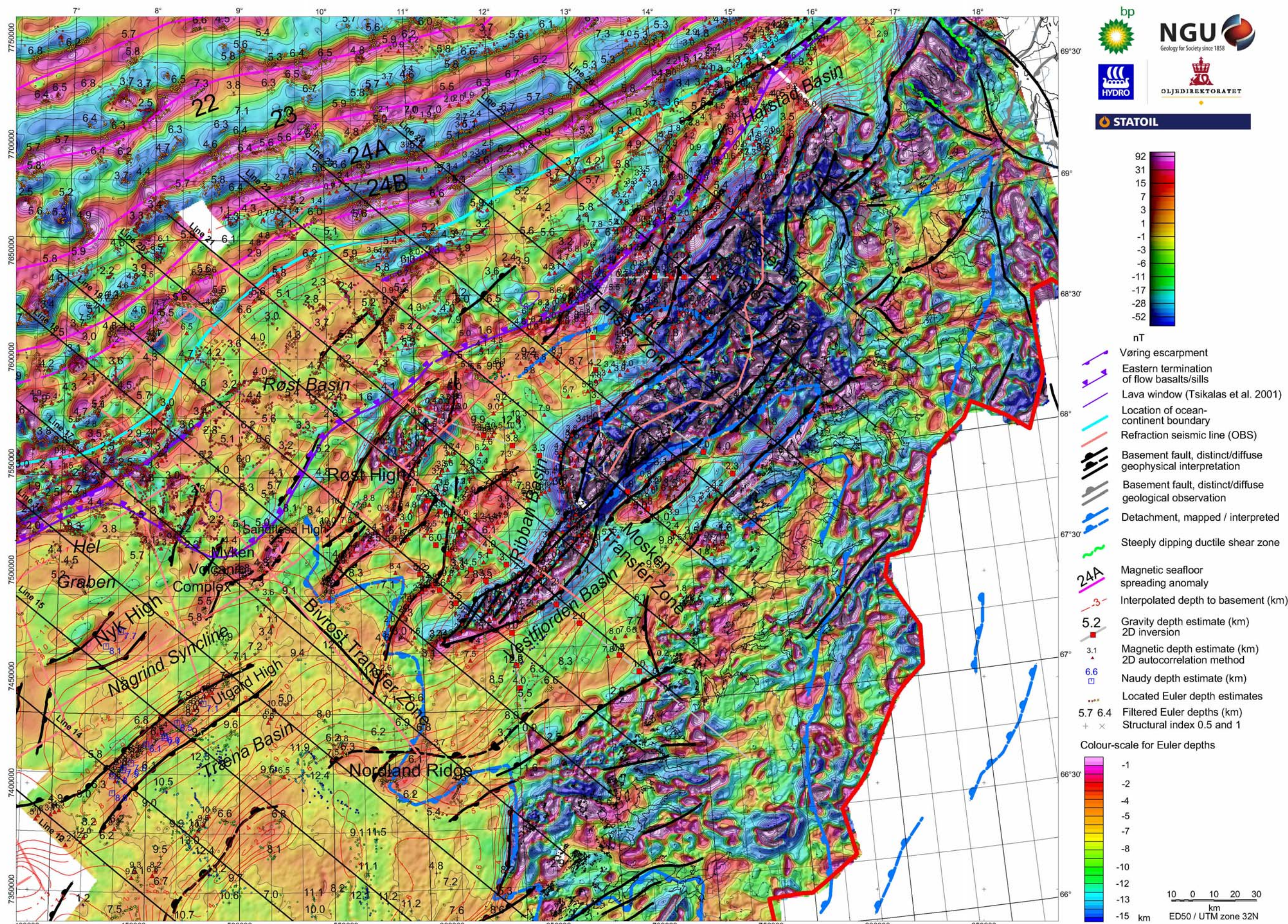


Figure 3.2 Aeromagnetic anomaly map, 25 km high-pass filtered, Nordland area

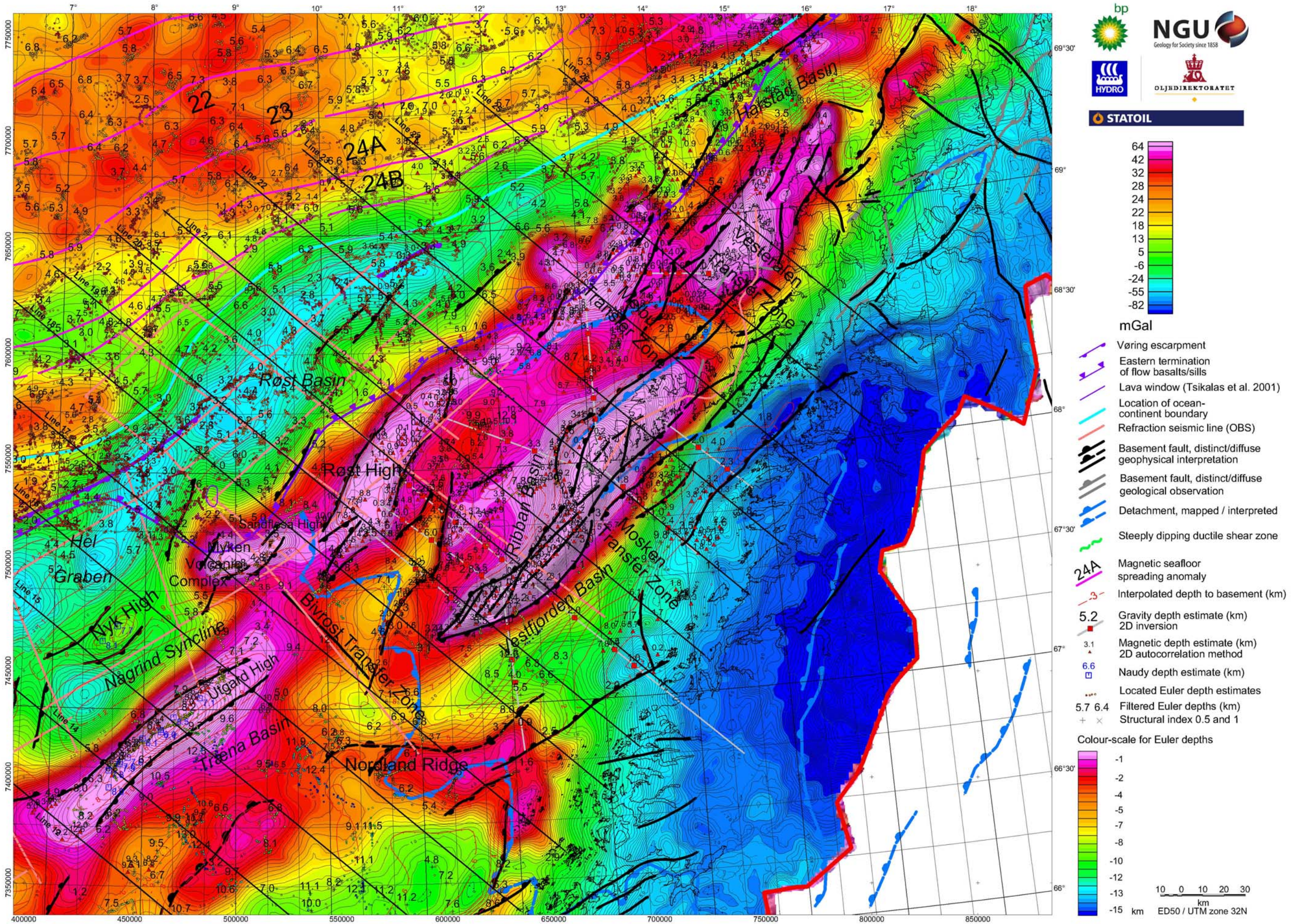


Figure 3.3 Free-air gravity map, Nordland area

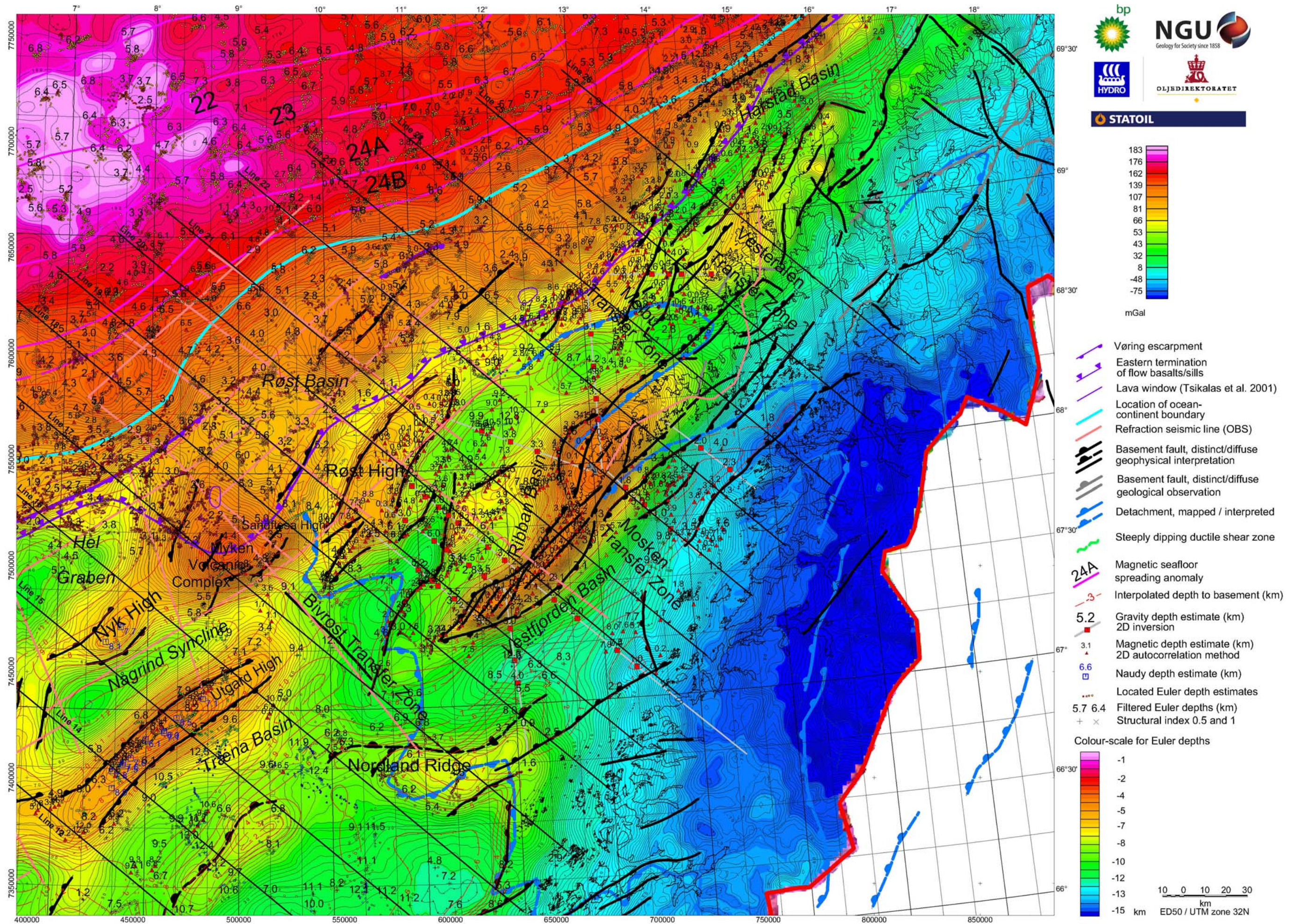


Figure 3.4 Bouguer gravity map, Nordland area

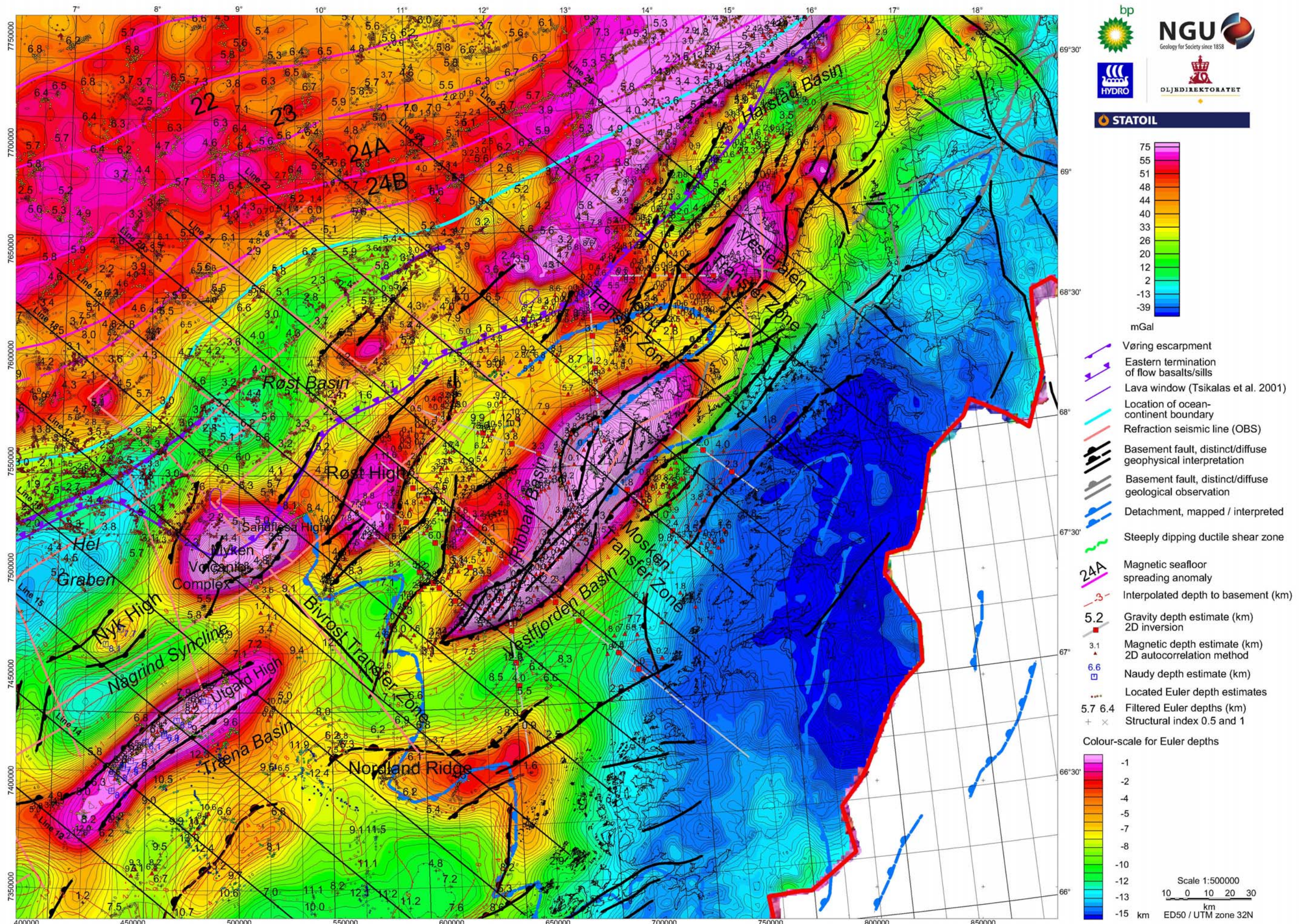


Figure 3.5 Isostatic residual, Bouguer gravity map, Nordland area

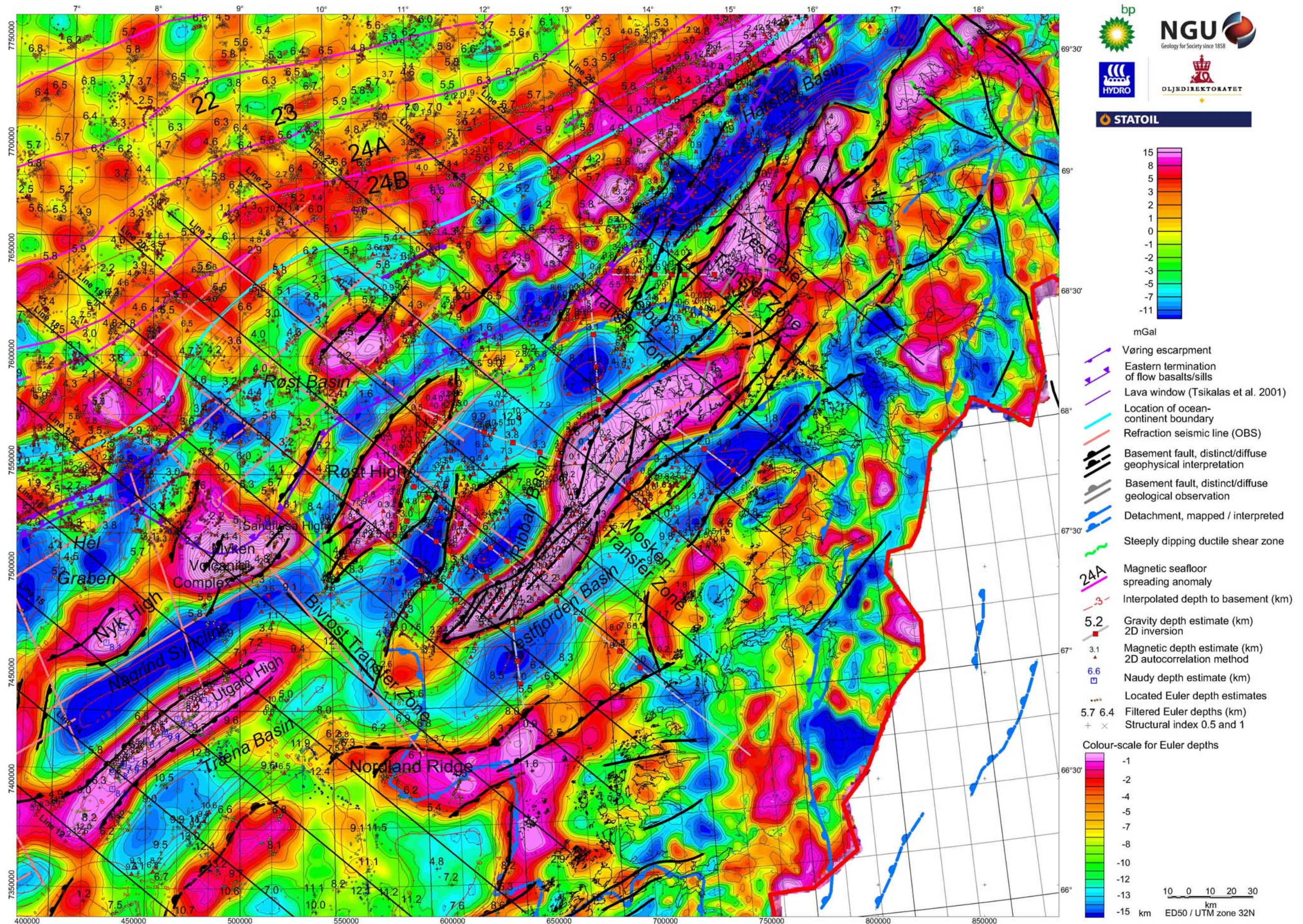
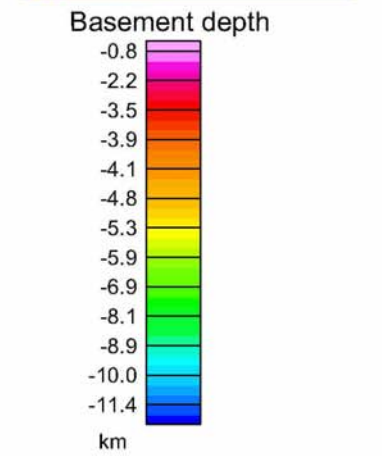












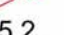






Figure 3.6 Bouguer gravity, 100 km high-pass filtered, Nordland area



-  Vøring escarpment
-  Eastern termination of flow basalts/sills
-  Lava window (Tsikalas et al. 2001)
-  Location of ocean-continent boundary
-  Refraction seismic line (OBS)
-  Basement fault, distinct/diffuse geophysical interpretation
-  Basement fault, distinct/diffuse geological observation
-  Detachment, mapped / interpreted
-  Steeply dipping ductile shear zone
-  Magnetic seafloor spreading anomaly
-  Interpolated depth to basement (km)
-  5.2 Gravity depth estimate (km) 2D inversion
-  3.1 Magnetic depth estimate (km) 2D autocorrelation method
-  6.6 Naudy depth estimate (km)
-  Located Euler depth estimates
-  5.7 6.4 Filtered Euler depths (km)
-  + x Structural index 0.5 and 1

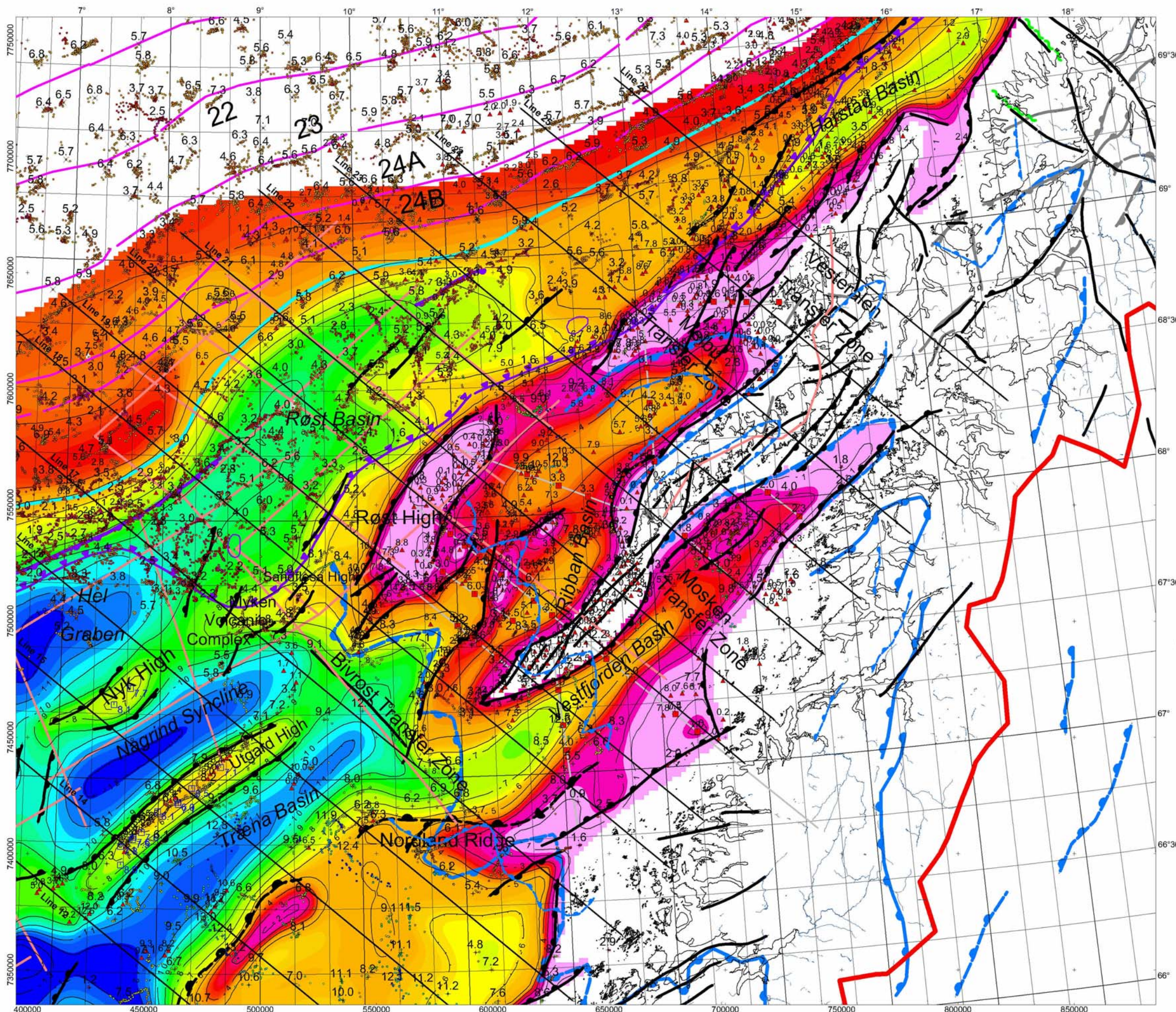
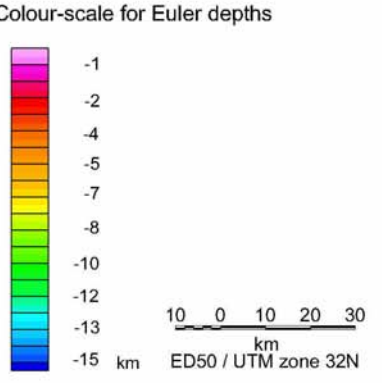


Figure 3.7 Geophysical interpretation map, Nordland area



#### 4 STRUCTURAL FRAMEWORK

The Lofoten continental margin has since post-Caledonian time been dominated by extensional tectonics. In the Devonian, the Caledonian nappes were dismembered by a late gravity collapse phase of the Caledonian orogen (Rykkelid & Andresen 1994, Braathen et al. 2000, 2002, Eide et al. 2002, Nordgulen et al. 2002 and Osmundsen et al. 2003). NW-SE trending detachment zones (Fig. 4.1) extending from the mainland, control the tectonic setting of the offshore Mesozoic basins. The entire Nordland mainland and offshore area is consequently affected by the NE-SW trending late Caledonian gravity collapse. The Nesna and Sagfjord shear zones (Osmundsen et al. 2000) extend north-westwards below the Helgeland, Vestfjorden and Ribban basins. The Bivrost Lineament most likely represents a detachment dipping 5-15° to the southwest and may constitute the offshore extension of the Nesna shear zone (Olesen et al. 2002). The structure consequently represents a rejuvenation of a much older zone of crustal weakness which also was suggested by Mokhtari & Pegrum (1992). Downfaulted low-magnetic Caledonian nappes most likely constitute the basement to the southwest of the Bivrost Lineament. The offshore extension of the Sagfjord shear zone may represent the initial crustal-scale fault zones on either side of the Lofoten and Utrøst Ridges. During subsequent regional extension the undulating detachment surface is interpreted to have been overprinted/utilized by the high-angle normal faults currently bounding the ridges [mapped by Mjelde et al. (1993) and Tsikalas et al. (2001)].

Late-Palaeozoic – Mesozoic rifting events have resulted in a shallow Moho and rotated fault-blocks separated by transfer zones giving rise to intermediate wavelength gravity and aeromagnetic anomalies. The positive gravity anomalies in the Lofoten-Vesterålen reflect mostly a shallow Moho discontinuity and uplifted, high-grade rocks of intermediate density (Svela 1971, Sellevoll 1983). The exhumation of the deep-crustal rocks in the Lofoten area has lately been interpreted as the exhumed lower plate of a core complex, denudated during large-magnitude extension along detachments in Permian time (Hames & Andresen 1996). Henkel & Eriksson (1987) and Gaal & Gorbatshev (1987) have interpreted the magnetite-bearing intrusive rocks in the Lofoten-Senja basement area and the Høgtuva-Sjona and Nasafjäll tectonic windows to be an integral part of the Transscandinavian Igneous Belt, which continues to the south and east beneath the magnetically transparent Caledonides into Sweden.

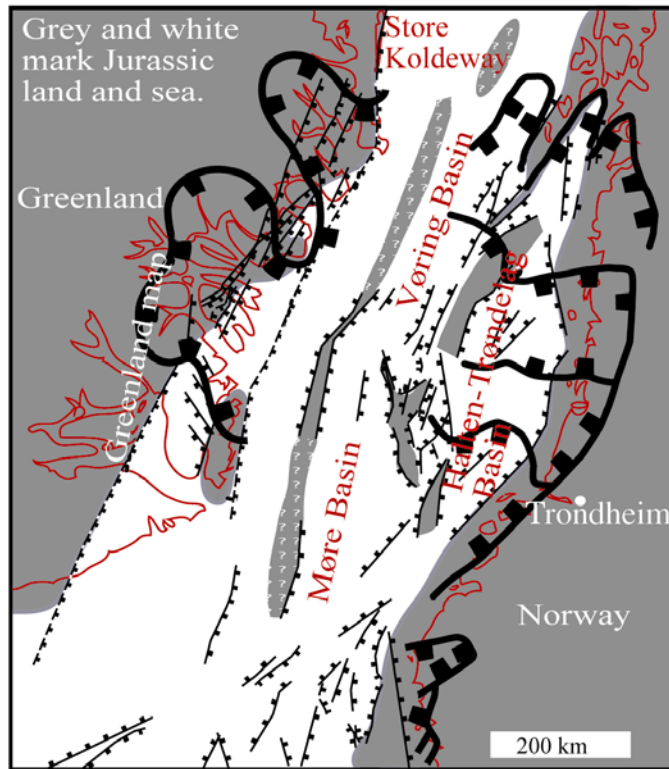


Figure 4.1 Sketch map of the main structural elements in the Norwegian-Greenland Sea area before opening of the Atlantic (Modified from Hartz *et al.* 2002, Braathen *et al.* 2002, Olesen *et al.* 2002 and Skilbrei *et al.* 2002). The bold black lines show the late Caledonian detachment zones.

Changes in Moho depths occur across the Surt, Bivrost and Vesterålen transfer zones indicating that these structures are continuous to great depths within the crust (Olesen *et al.* 2002). The more local Mosken and Melbu transfer zones separate structural domains characterised by different fault-polarities within the Ribban and Vestfjorden basins. The Harstad Basin (Gabrielsen *et al.* 1990) extends from offshore Andøya northeastwards to the west of the islands of Senja, Kvaløya and Ringvassøya. A set of steep semi-ductile to cataclastic faults called the Vestfjorden-Vanna fault complex (Andresen & Forslund 1987) continues from the Vestfjorden area through the sounds to the east of Hinnøya, Senja and northwards. The major NNW-trending Bothnian-Senja fault complex (Henkel 1991, Zwaan 1995, Olesen *et al.* 1997b) can be observed on Senja and Kvaløya on either side of Malangen. The Vestfjorden-Vanna fault complex changes polarity at both intersections with two segments of the Bothnian-Senja fault complex (Olesen *et al.* 1997b).

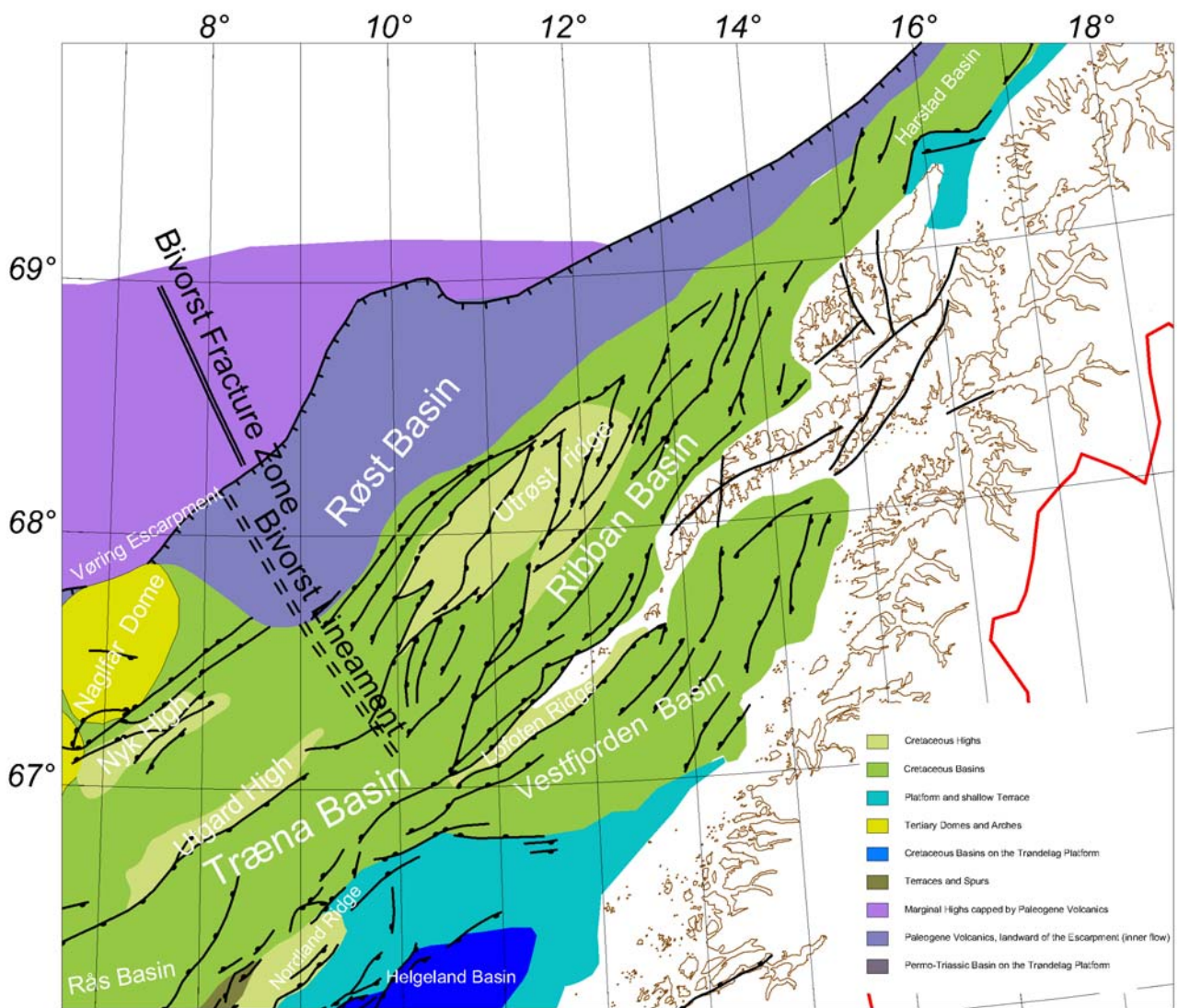


Figure 4.2 Main structural elements in the Nordland area (Blystad *et al.* 1995).

Seaward the Utrøst Ridge is bound by major normal faults (Mokhtari & Pegrum 1992, Mjelde *et al.* 1992) with northwest throws, forming the landward boundary of the basalt-covered Røst Basin. Evidence of a sub-basalt sedimentary sequence is based on data derived from inversion of gravity data (Sellevoll *et al.* 1988), ocean bottom seismographs (Mjelde *et al.* 1992) and forward gravity modelling (Olesen *et al.* 1997b). The interpreted thickness of the volcanics varies from rather thin (less than 500 m, Sellevoll *et al.* 1988) up to 2.5-3 km (Mjelde *et al.* 1992). The lower part of the thick volcano-sedimentary package may represent sills (Mjelde *et al.* 1992). Based on seismic volcanostratigraphy Berndt *et al.* (2001) identified the volcanic emplacement environment on the Norwegian margin. The Lofoten-Vesterålen margin constitutes one of the five identified provinces on the margin and is characterized by four different facies units: 1) Lofoten margin flows, 2) Outer highs, 3) Outer seaward dipping reflectors (SDR), and 4) a Tuff sheet in the upper part of the Myken volcanic complex. The Lofoten margin flow is the

innermost unit and covers the Røst Basin westwards to the Outer SDR. The flows were according to Berndt et al. (2001) deposited in a deep marine environment while Tsikalas et al. (2001, 2002) seem to propose a shallow marine or sub-aerial deposition. In the very southeastern part of the Lofoten-Vesterålen margin the flow basalts disappear underneath the proposed tuff sheet.

Tsikalas et al. (2001) have interpreted two lava windows and a volcanic mound within the flood basalt area. They have also interpreted bulbous-shaped deviations in the easternmost boundary in the area to the west of the Jenegga High. These results differ significantly from the interpretations by Blystad et al. (1995) who interpreted a more linear termination of the easternmost lava-front.

The continent-ocean boundary (COB) has been interpreted through the area (Sellevoll et al. 1988, Blystad et al. 1995). Previous interpretations of the continuation of the Vøring Escarpment into the Røst Basin vary to a large degree. The location of the Vøring Escarpment by Sellevoll et al. (1988) and Mjelde et al. (1992) coincides with a sharp westward deflection in the COB. Tsikalas et al. (2001) and Berndt et al. (2001), on the other hand, have interpreted a linear continent-ocean transition zone (COT) and a gap in the Vøring Escarpment along the western margin of the Røst Basin. The Vøring escarpment corresponds to a paired negative and positive anomaly with values of  $-300$  nT on the landward side of the escarpment and small,  $0-50$  nT, positive values on the seaward side. The anomaly can be modelled by the superposition of an upper series of normally magnetised flood basalts and an underlying reversely magnetised series (Roeser 1993, Olesen & Skilbrei 1993, Tsikalas et al. (2002). The escarpment represents most likely a coastline lava front (e.g. Brekke 2000). The COT decreases in width from 50 km in the Røst Basin to approximately 30 km offshore Andøya (Tsikalas et al. 2002).

A high-velocity lower crustal body, generally accepted to represent underplated material of assumed Late Palaeocene age occurs below the Vøring Basin. This velocity anomaly extends southeastward into the Nordland area and tapers out to the north across the Bivrost Lineament (Planke et al. 1991; Mjelde et al. 1998).

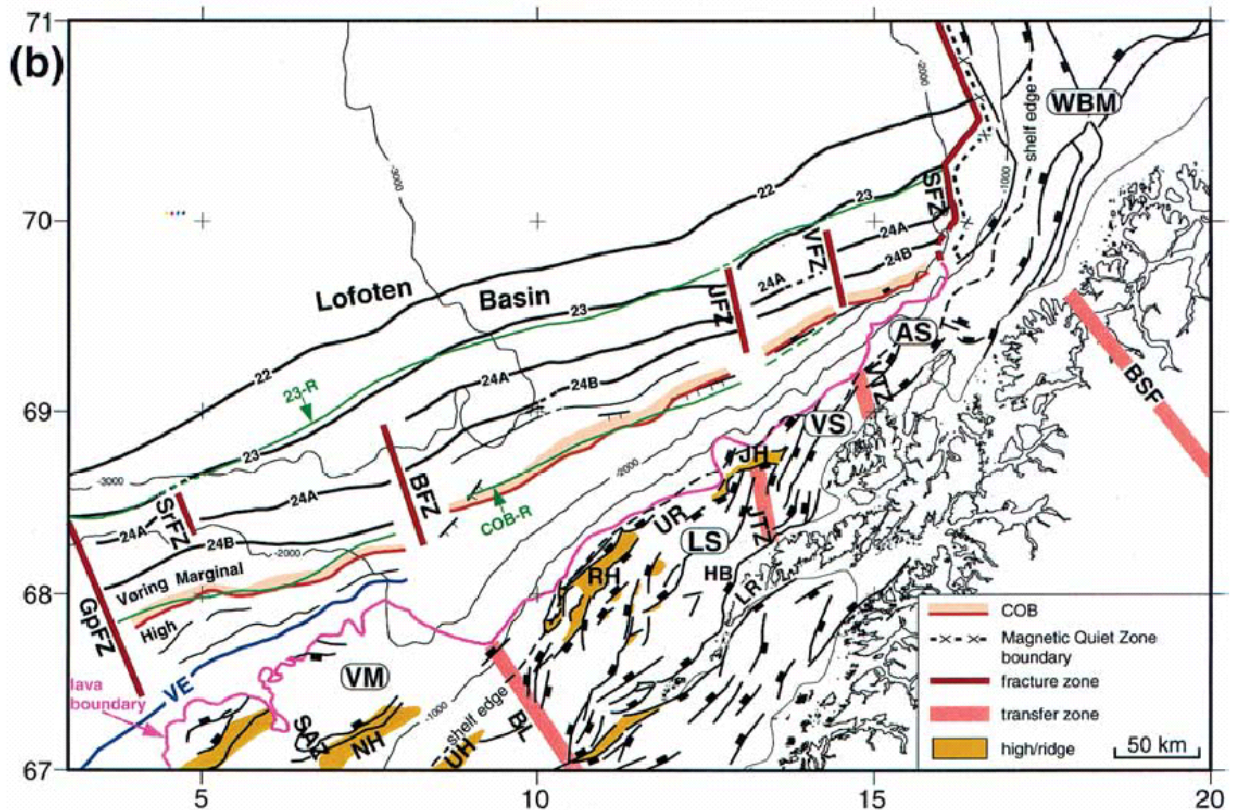


Figure 4.3 Magnetic lineations and structural elements off Norway (Tsikalas et al. 2002). LS, VS, AS, Lofoten, Vesterålen, and Andøya margin segments, respectively; SAZ, Surt accommodation zone; NH, UH, RH, JH, Nyk, Utgard, Røst, and Jennegga highs, respectively; LR, UR, Lofoten and Utrøst ridges, respectively; HB, Havbåen sub-basin. 23-R and COB-R are conjugate features rotated from the Greenland margin.

The sea-floor spreading magnetic anomalies 22-24B (Talwani & Eldholm 1977; Eldholm et al. 1979; Hagevang et al. 1983) are revealed in the northwesternmost part of Figs. 3.1 - 3.2. Anomalies 24 A and 24 B refer to Chron 24n.1n (52.51 Ma) and 24n3n (53.13 Ma), respectively (Cande & Kent 1995). Various NNW-SSE oriented oceanic fracture zones have previously been interpreted in the Nordland-Troms area: the Bivrost, Jennegga, Vesterålen and Senja fracture zones (Hagevang et al. 1983, Blystad et al. 1995, Tsikalas et al. 2001). The previously interpreted offset along the Bivrost fracture zone varies from 50 km by Blystad et al. (1995) to 40 km by Tsikalas et al. (2002), 15 km by Hagevang et al. (1983) and 10 km by Olesen et al. (2002). The apparent offset along the Jennegga fracture zone varies from 3 km (Olesen et al. 1997b, 2002) to 5-6 km (Tsikalas et al. 2001). Notably, Tsikalas et al. (2001) placed the Jennegga fracture zone 50 km north of earlier interpretations and interpreted a 5-6 km offset along the Vesterålen fracture zone further north. Olesen et al. (2002) argued that the large variation in interpretations is partly due to the wide line spacing and low quality of navigation and levelling of the previous aeromagnetic surveys. Tsikalas et al. (2002) applied the aeromagnetic compilation of Verhoef et al. (1996) consisting of a 5 x 5 km grid. The grid cell

size is consequently in the same order as the interpreted offsets. Tsikalas et al. (2002) have correlated the three “fracture zones” on the Lofoten margin with similar apparent breaks in the spreading anomalies 24 A and B on the conjugate Greenland margin where the line spacing (10-20 km) is larger than for most areas along the Norwegian continental margin (4-15 km line spacing). Since the fracture zones on the Norwegian margin do not appear to be real features, but relate to data problems, we question the existence of the correlative NE Greenland fracture zones. Fig. 4.2 shows the main offshore structure elements in the offshore Nordland area (from Blystad *et al.* 1995).

## 5 RESULTS

### 5.1 3D gravity model

The two parameters most important for constructing the 3D density model are the geometry and the density of the structures. The densities used in the modeling are based on published values (Mjelde et al. 1998, Olesen et al. 2002, Olesen and Smethurst 1995, Olesen and Torsvik 1993) listed in Table 2.5. The densities from the deep parts of the basins are based on velocity-density relationships (e.g. Ludwig et al. 1970).

In addition to the density structure of the crust (as described below) the lithospheric mantle was modelled by assuming a stepwise increase (200°K) in temperature from the Moho (c. 500°C) to the asthenosphere at a temperature of c. 1300 °C. Therefore a thermal expansion factor of  $3.2 \times 10^{-5} \text{ K}^{-1}$  was applied, adapted from studies by Breivik et al. (1999) for the Barents Sea and from Olesen et al. (2002) for the Nordland offshore area.

The modelled cross-sections (Figs. 5.4 - 5.13) show some distinctive features, described in the following sections. The adjustment of the modelled gravity to the observed gravity anomalies is generally good. Only minor misfits remain, and relate to the resolution of the model. The gravity field is strongly influenced by the geometry of the Moho (Fig. 5.1), the existence of magmatic underplated material, the crustal density and the thickness of sediments.

### 5.1.1 Moho geometry and magmatic underplating

The cross sections south of the Bivrost Lineament feature a body of magmatic underplated material (Profiles 14 – 17 in Figs. 5.4 – 5.7). The existence of magmatic underplating is constrained by a variety of OBS studies in the northern and central Vøring Basin (e.g. Mjelde et al. 1998). The south-eastern boundary of the magmatic underplating coincides with an upward-facing Moho bulge (Fig. 5.1) below the Utgard High.

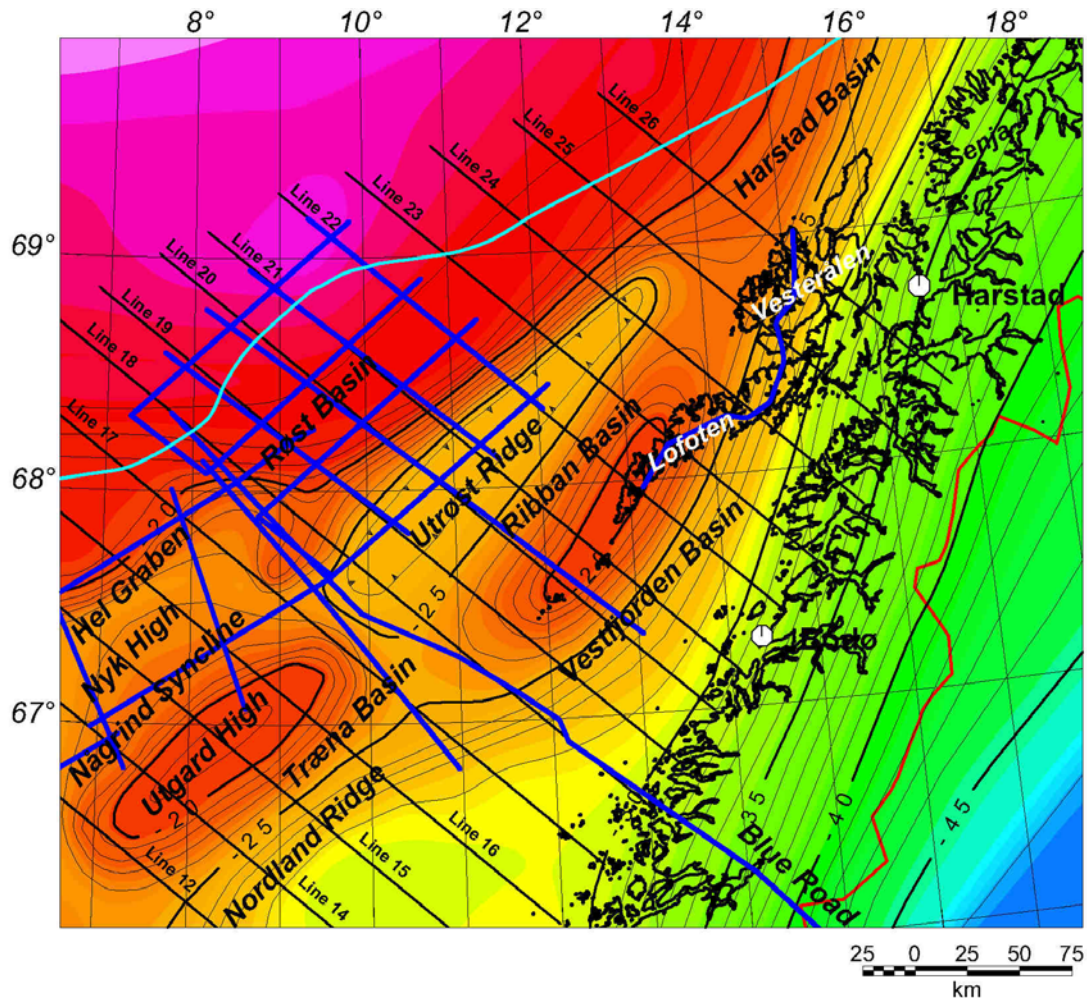


Figure 5.1. Depth to Moho compiled from refraction seismic studies (Lund 1979, Kinck et al. 1993, Mjelde et al. 1992, 1993, 1997, 1998, Sellevoll 1983) and gravity interpretations (Olesen et al. 1997, 2002). The black lines show the interpreted profiles within the present 3D model. Blue lines show the refraction seismic lines. The pale blue line denotes the interpreted continent-ocean boundary.

The underplated material tapers out to the northeast at the Bivrost Lineament (Profile 17 in Fig. 5.7) and the Moho below the Røst Basin is c. 15 km deep (compared to 20 km below the Hel Graben and Nâgrind Syncline). Landward from the Røst Basin, the Moho depth is c. 25 km below the Røst High and Ribban Basin (Figs. 5.8 - Fig 5.13). Further landwards the

Moho shallows to 20 km below the Lofoten Ridge. An analogous Moho shallowing occurs below the Utgard High (described in later sections). The Moho deepens further towards the Norwegian mainland, where it can be found at a depth of 27-30 km.

### 5.1.2 Crustal density

Important features of the 3D density model are the different densities in the basement and lower crust on either side of the Bivrost Lineament. In the Lofoten area, north of the Bivrost Lineament, the basement has a density of 2700-2750 kg/m<sup>3</sup> and the lower crust a density of 2950 kg/m<sup>3</sup> (e.g. Profiles 19 & 20 in Figs. 5.9 & 5.10, respectively). To adjust the anomalies north and south of the Bivrost Lineament the density in the basement in the southern part of the model had to be increased to 2850 kg/m<sup>3</sup>. The density of the lower crust east of the Utgard High is 2.95 gr/cm<sup>3</sup>, but west of it, above the magmatic underplated body the density had to be increased to 3000 kg/m<sup>3</sup> (e.g. Profiles 14 - 16 in Figs. 5.4 - 5.6). This could possibly relate to mafic intrusions with high density. Berndt et al (2000) have described sills in the Hel Graben and Någrind Syncline with velocities above 7 km/s.

### 5.1.3 Depth to basement

The crustal densities and the geometry of the Moho are mainly causing the long wavelength changes in the gravity field. The geometry of the sedimentary basins and the basement depth also affect the long-wavelength anomalies, but usually only add medium- to short-wavelength components to the gravity field. South of the Bivrost Lineament, the basement is deeper than to the north. The geometry is characterized by an undulating surface, changing from deep basement in Hel Graben, Någrind Syncline, and Træna Basin to shallow basement at the Nyk and Utgard Highs. All these structures are well expressed in the basement depth surface, which ranges from a maximum of 12 km in Hel Graben to a minimum of 2-3 km on the Nordland Ridge. North of the Bivrost Lineament, the basement relief is even rougher and at the Lofoten Ridge basement rises northward, forming a nearly 8 km high ridge (Profiles 18 - 21, Figs. 5.8 - 5.11). Below the Røst Basin the basement depth can be up to 10 km, but further landwards the depth ranges between c. 5 and 0 km. The abrupt changes in the basement depth are the cause of the more high-frequency anomalies in the gravity field north of the Bivrost Lineament. The Myken volcanic complex on Profile 17 (Fig. 5.7) is interfering with the basement surface (see section 5.4.2 below).



## 5.2 3D magnetic structure

The 3D structure of the density model was also interpreted and adjusted to the magnetic signature of the study area. The fit of the modelled magnetic anomaly to the observed anomaly is not as good as for the gravity field. However, the main focus was on modelling the gradient of the magnetic field, and not on modelling the amplitudes perfectly. The gradient is most sensitive to the depth of the magnetic sources. An improved fit to the observed magnetic anomalies can only be achieved through a more detailed 3D model, which due to the increased number of cross sections would provide higher resolution. In order to model the magnetic field, some adjustments/refinement of the gravity model had to be done. First of all the depth of the Curie temperature had to be included in the model.

### 5.2.1 Curie temperature

The magnetic data will only reveal information for the part of the model, which has a present temperature below the Curie temperature. Rocks at higher temperatures will not show the ferromagnetic behaviour necessary to generate the discernible magnetic signal. The dominant magmatic material is regarded to be magnetite, which has a Curie temperature of 580 °C (cf. Hunt et al. 1995). The depth to the Curie temperature is estimated to be 12.5 km at the COB, and linearly deepening landwards to 22.5 km below the coastline. These values correspond to a constant temperature gradient from the surface to the Curie depth of 45 °C/km at the COB and 25 °C/km at the coastline. These values represent a typical range for continental shelf and oceanic crust. The estimate of the depth to the Curie-temperature is consistent with previous studies from the Lofoten area and the Vøring Basin (Fichler et al. 1999). The comparison between the Curie depth and the model shows that the border between magnetic and non-magnetic material generally runs through the lower continental and oceanic crust. The modelling of the magnetic anomalies shows that there are mainly two features causing the magnetic signatures: basement and volcanic rocks.

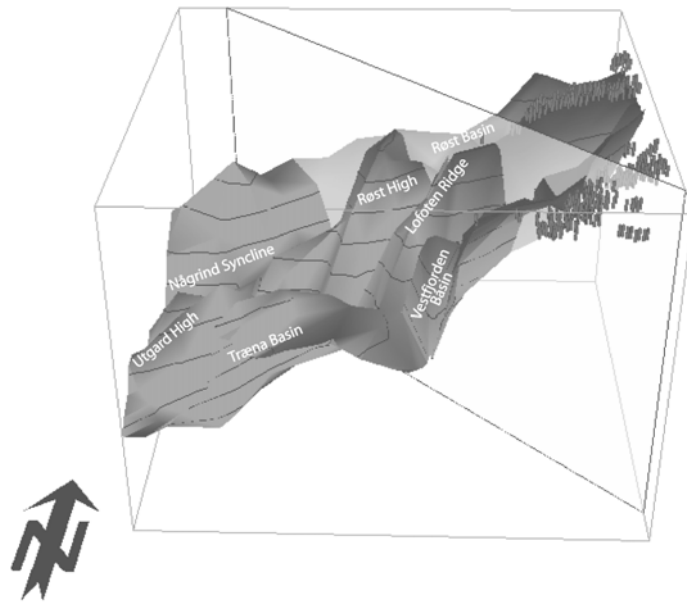


Figure 5.2 3D perspective map of the basement in Nordland area (seen from the south).

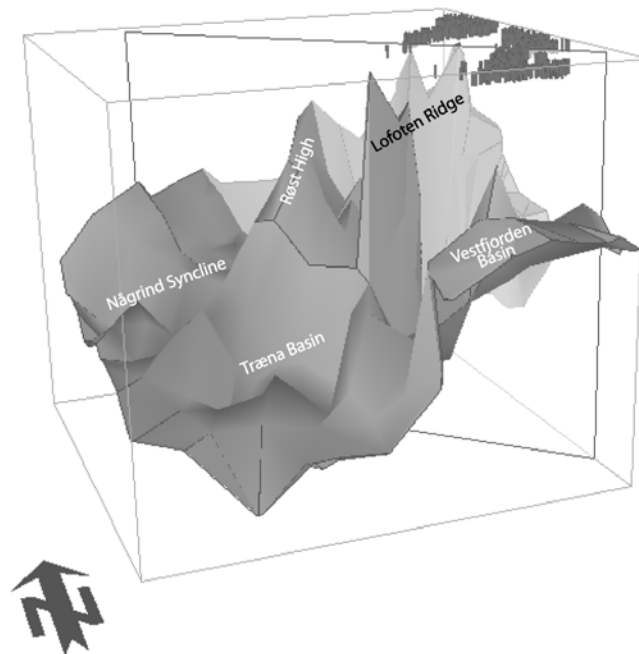


Figure 5.3 3D perspective map of the magnetic basement in Nordland area showing that there is a substantial amount of low-magnetic basement rocks below the deepest part of the Vestfjorden, Træna and Ribban basins in addition to the Nordland Ridge (view from the southwest).

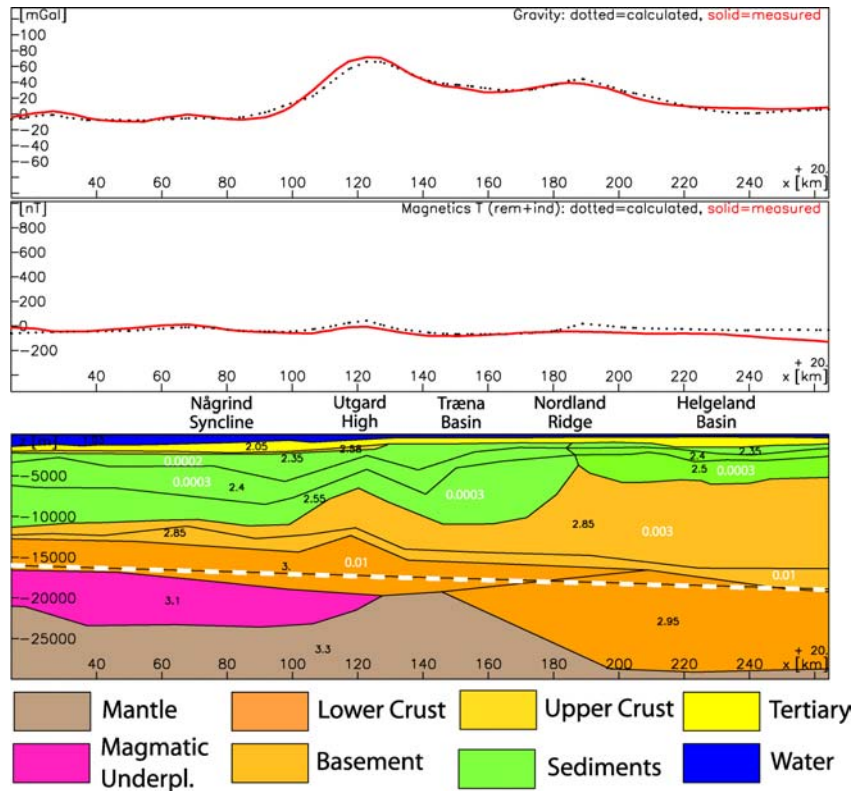


Figure 5.4 Profile 14 of the 3D model. The upper panel shows the gravity anomaly (offshore: Free-Air anomaly, onshore: Bouguer anomaly), the middle panel the magnetic anomaly and the lower panel the modelled density/magnetic cross-section. Black numbers are density values in  $\text{gr}/\text{cm}^3$ , white numbers represent magnetic susceptibilities. The black-white dotted line indicates the Curie depth. See Figs 3.1 - 3.7, 5.15 and Maps 1 - 7 for exact location of the profile and text for further details.

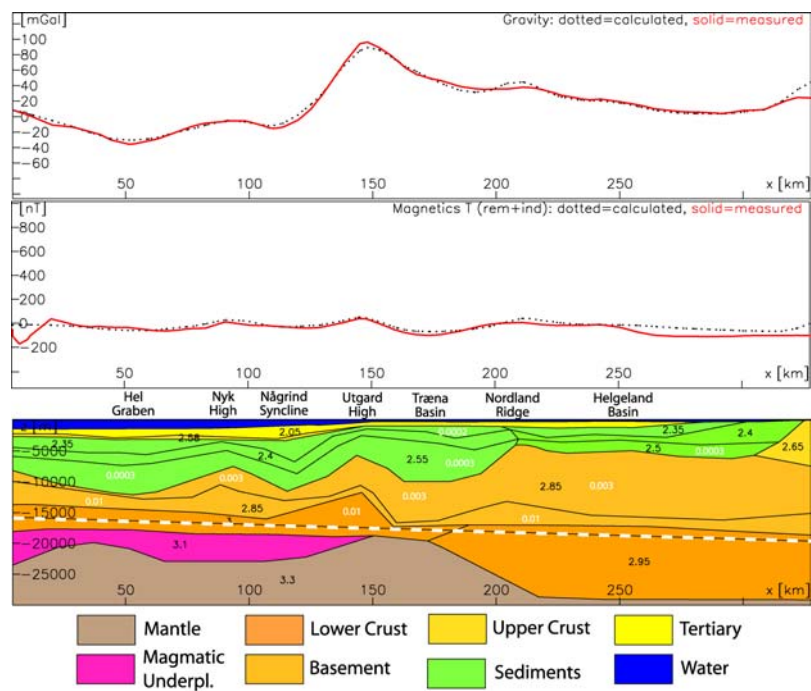


Figure 5.5 Profile 15 of the 3D model. See description of Fig. 5.4 for further details.

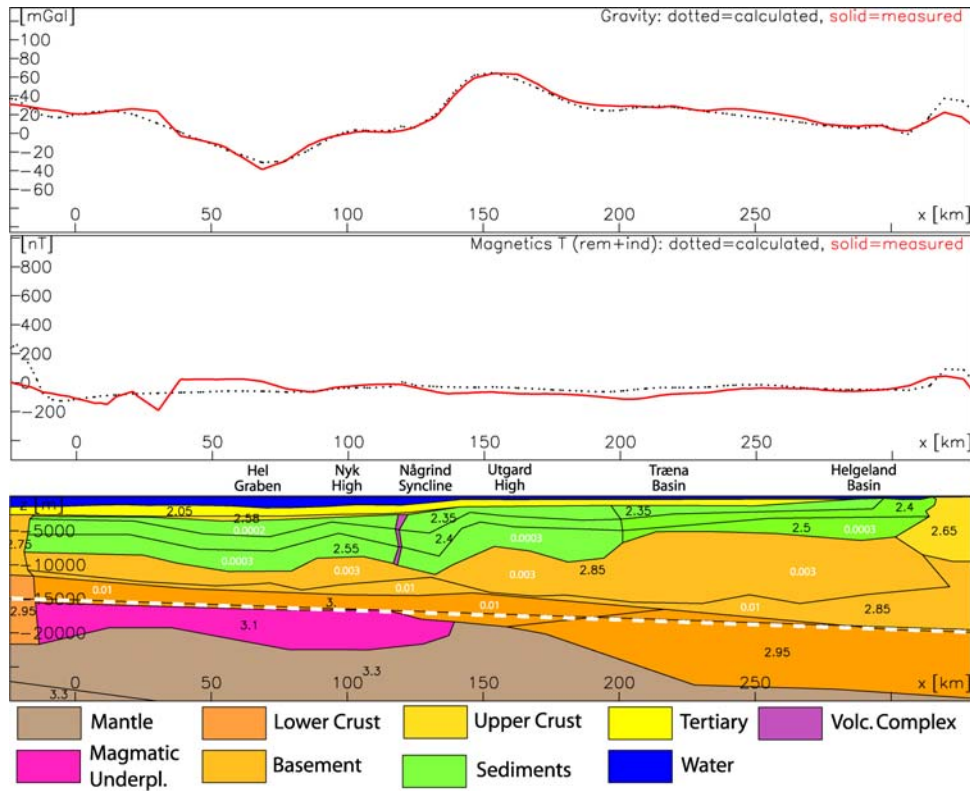


Figure 5.6 Profile 16 of the 3D model. See description of Fig. 5.4 for further details.

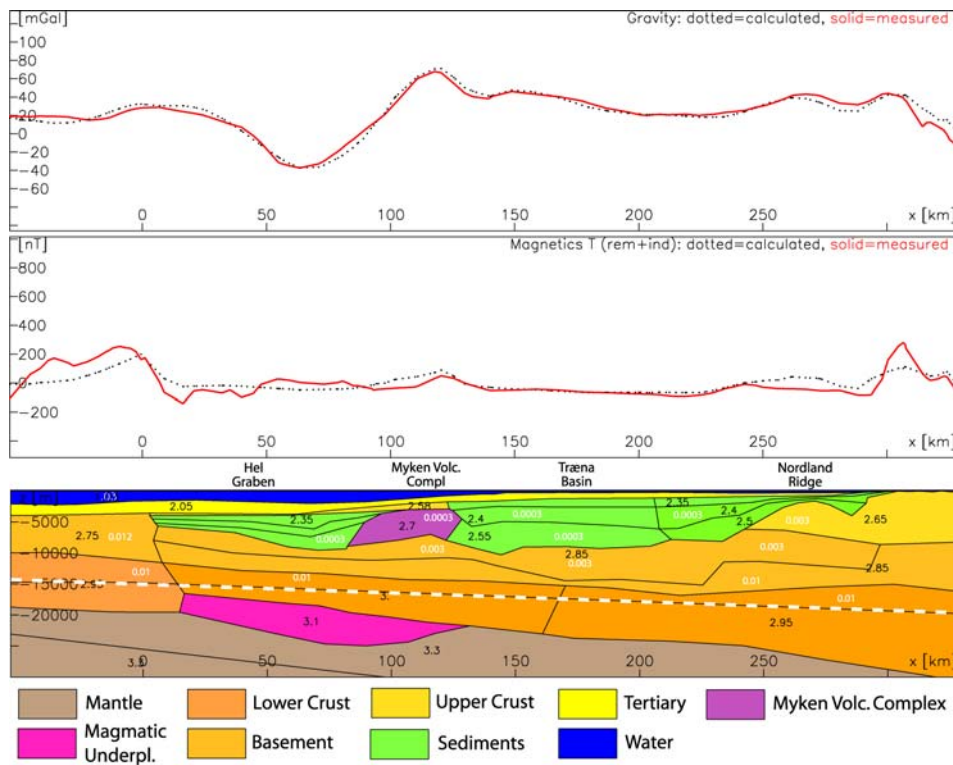


Figure 5.7 Profile 17 of the 3D model. The location of the profile is close to the assumed location of the Bivrost Transfer Zone. The Myken Volcanic Complex in the central part of the profile is causing a prominent gravity anomaly. See description of Fig. 5.4 for further details.

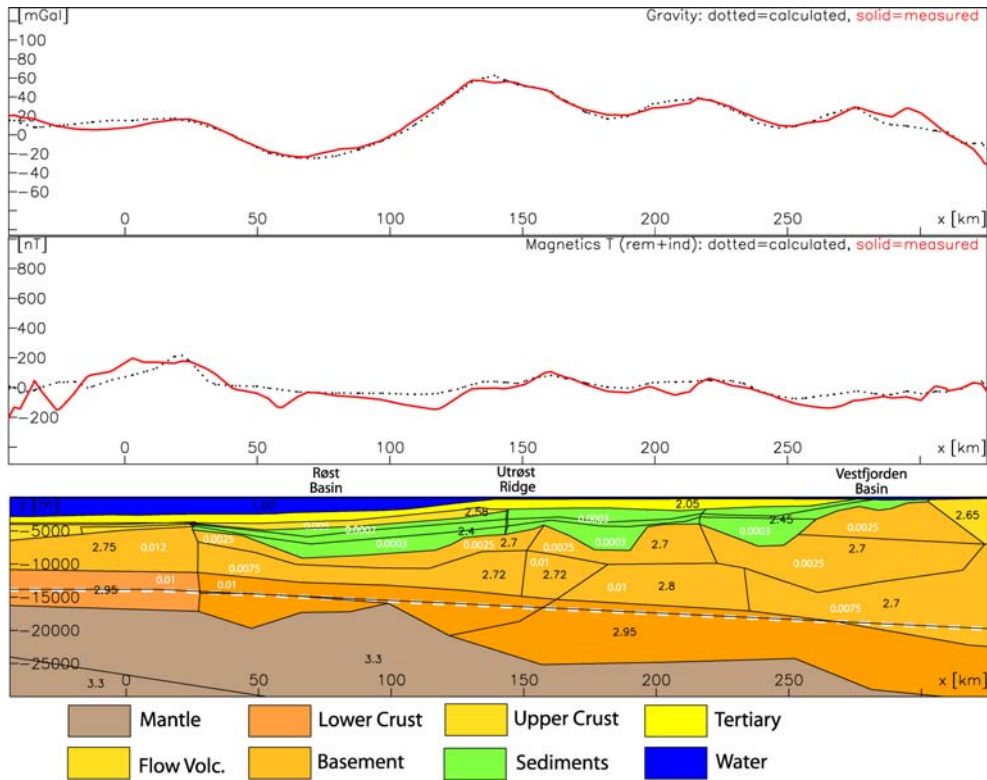


Figure 5.8 Profile 18 of the 3D model. The profile is the first immediately to the north of the Bivrost Lineament. See description of Fig. 5.4 for further details.

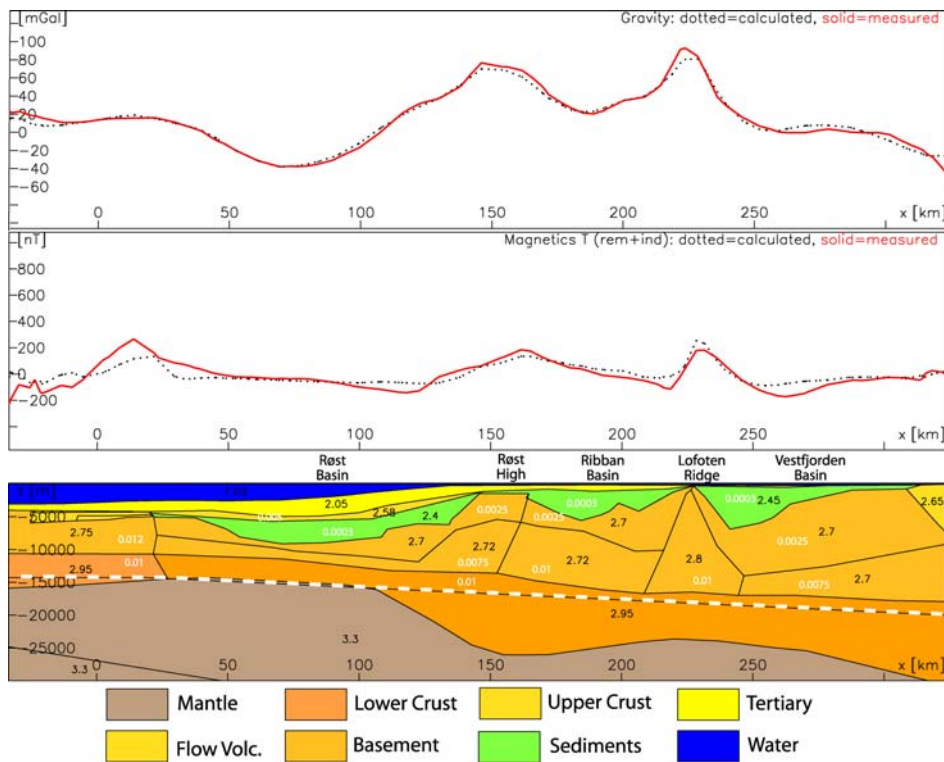


Figure 5.9 Profile 19 of the 3D model. The location of the line is coinciding with the OBS line 2 (Mjelde et al. 1992). See description of Fig. 5.4 for further details.

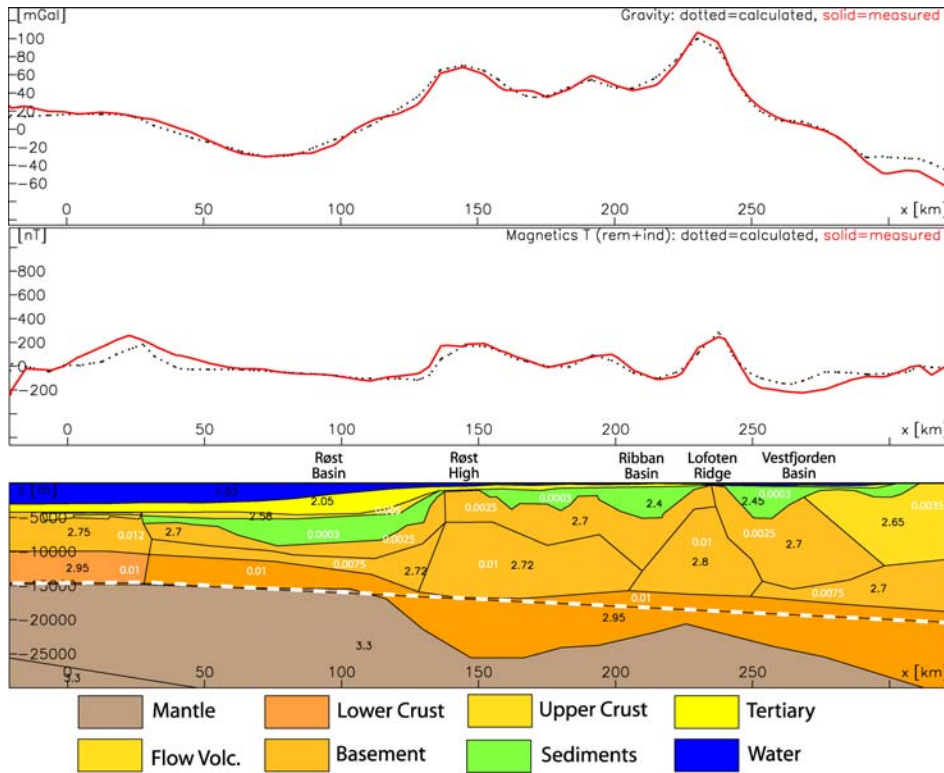


Figure 5.10 Profile 20 of the 3D model. The location of the line is coinciding with OBS Lines 1 and 3 (Mjelde et al. 1992). See description of Fig. 5.4 for further details.

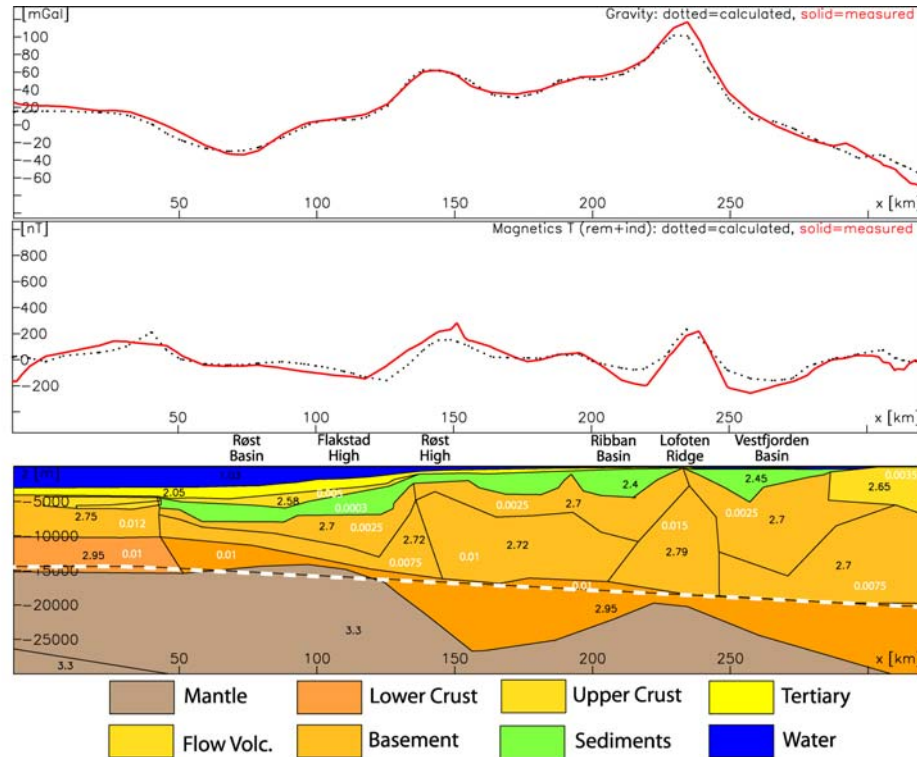


Figure 5.11 Profile 21 of the 3D model. The location of the line is coinciding with OBS Line 4 (Mjelde et al. 1992). The Flakstad High is one of the new tectonic structures identified by the new data compilations. See description of Fig. 5.4 for further details.

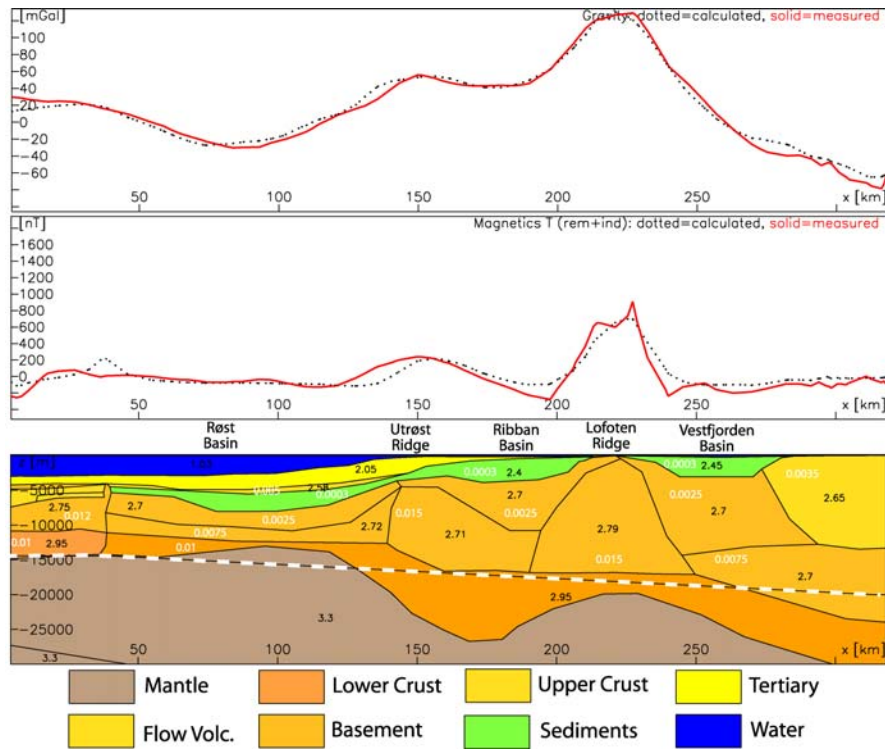


Figure 5.12 Profile 22 of the 3D model. The location of the line is coinciding with OBS line 5 (Mjelde et al. 1992). See description of Fig. 5.4 for further details.

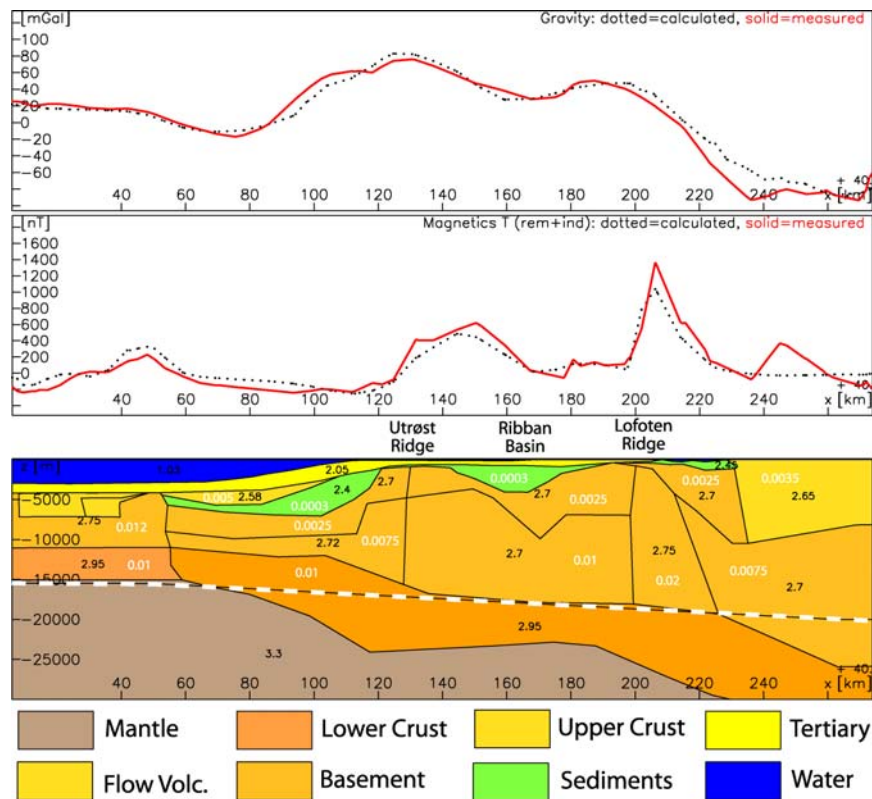


Figure 5.13 Profile 24 of the 3D model. On this profile the magnetic signature over the Lofoten Ridge has a maximum of 1500 nT. See description of Fig. 5.4 for further details.

### 5.2.2 Magnetic basement

The main magnetic material is expected to be in the basement, while the overlying sediments have only a small magnetic contribution. Susceptibilities of the basement can range between 0.001 and 0.02 SI (with Königsberg ratios between 1-4) while susceptibilities of the overlying sediments are in the order of 0.0003 SI. The main magnetic signature is therefore, caused by the changing geometry between the low- and the high-magnetic basement. The inclination and declination of all remanent fields is set to 77.0° and 0.5°, approximately parallel to the present magnetic field, when not mentioned otherwise. As in the gravity interpretation, the crustal and basement characteristics north and south of the Bivrost Lineament vary. South of the Bivrost Lineament the magnetic anomalies range between -200 and +200 nT, while the magnetic signature in the Lofoten area varies between -300 and 800 nT, with peaks up to 1600 nT. To model these different characteristics of the magnetic field, the basement is generally assigned low magnetic susceptibility in the south and higher magnetic susceptibility in the north.

Figs. 5.4 - 5.7 show the cross-sections (Profile 14 - 17) to the south of the Bivrost Lineament. The upper part of the basement has low susceptibilities (0.0025 SI), while the lower basement has a higher value (0.0075 SI). The modelling shows that the transition between high and low magnetic materials occurs at a depth of 10 km at the ocean-continent transition and at a depth of 15-18 km along the coastline. The border between high- and low-magnetic basement shows small undulations, but in general only the lowermost part of the basement can have high susceptibilities (2.5 km above the Curie depth).

North of the Bivrost Lineament the characteristics of the basement change rather quickly. Fig. 5.8 (Profile 18) still shows a characteristic similar to profiles south of the Bivrost Lineament, but along Profile 19 (Fig. 5.9) the basement shows two regions of higher susceptibilities (0.01), below the Røst High and Lofoten Ridge. Further to the north (Fig. 5.10 – 5.13) the susceptibilities increase up to 0.02 and the high-magnetic basement reaches nearly the surface. Between the Røst High and the Lofoten Ridge, the transition to the high-magnetic basement is at a depth of 7 to 13 km. This leads to edgy, abrupt changes lateral and vertical boundaries between low- and high-magnetic material and is causing the steep gradients of the magnetic anomalies.



### 5.3 Oceanic magnetic anomalies

In addition to the geometry of the magnetic basement a second feature has to be mentioned, which is connected to the COB. At the COB the remanent anomalies connected to the sea-floor spreading are visible (Figs. 3.1, 3.3, 3.7, 5.14 & 5.15, Maps 1, 2 & 7). These anomalies are due to remanent magnetisation of oceanic basement material. The oceanic basement in the models has a susceptibility of 0.012 and the inclination and declination of the remanent fields is set to 77.0° and 0.5°, as for the rest of the model. But the remanent anomalies connected to the sea-floor spreading formed during reversals of the Earth's magnetic field (i.e. both during normal polarity as today and periods of reversed polarity).

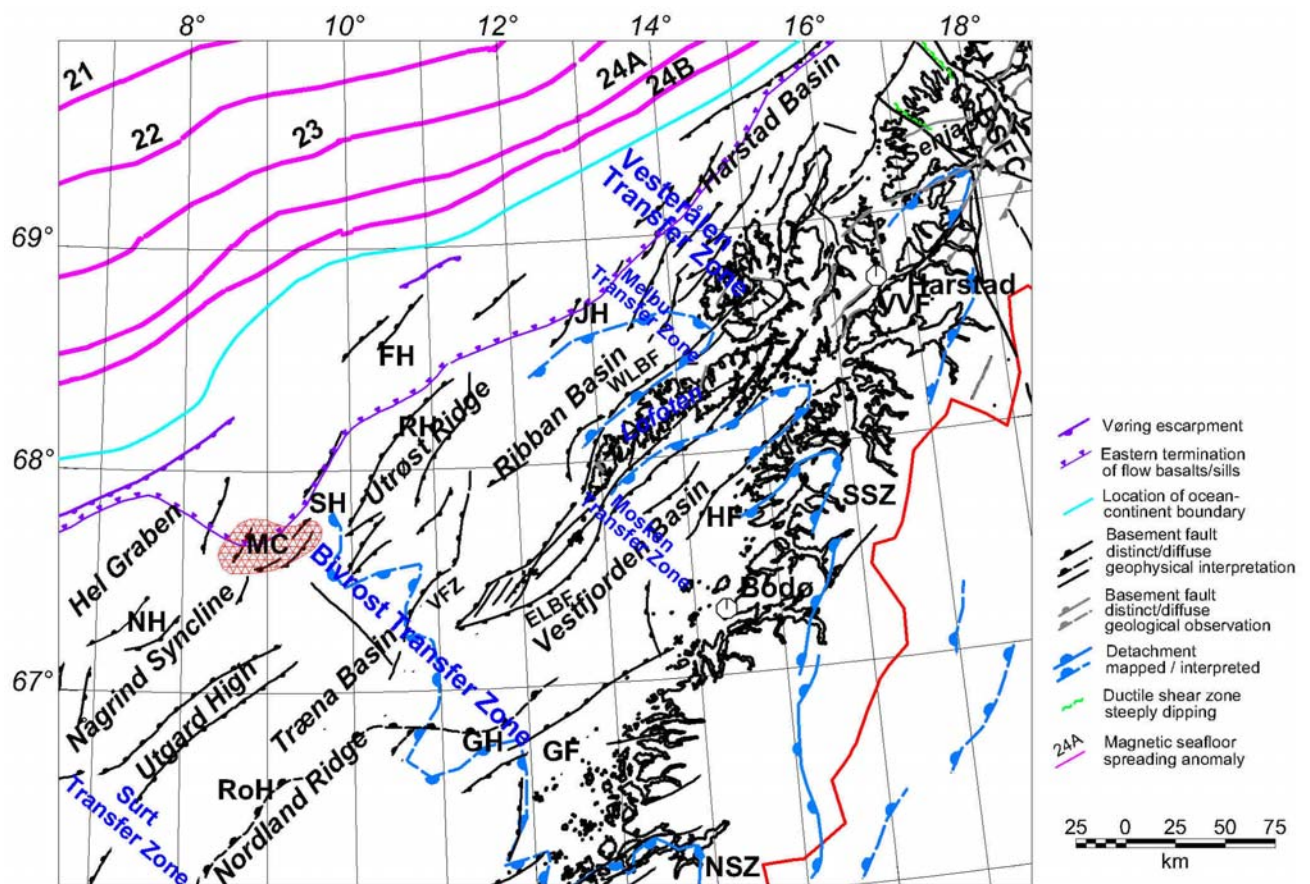


Figure 5.14 Regional basement faults within Nordland area. GF - Grønna fault, HF - Hamarøya fault, NSZ - Nesna shear zone, SSZ - Sagfjord shear zone; FH - Flakstad High; JH - Jennegga High; SH - Sandflesa High; RH - Røst High; NH - Nyk High; RoH - Rødøy High; GH - Grønøy High; VFZ - Vesterdjupet Fault Zone; BSFC - Bothnian-Senja fault complex; VVF - Vestfjorden-Vanna fault complex; WLBF - Western Lofoten border fault; ELBF - Eastern Lofoten border fault; MC - Myken volcanic complex. The nomenclature is adapted from Andresen & Forsslund (1987), Blystad et al. (1995), Løseth & Tveten (1996), Olesen et al. (1997b), Tsikalas et al. (2001) and Braathen et al. (2002).

Therefore, to model the magnetic seafloor spreading anomalies a remanent magnetic body was placed in the lower crust with an inclination of  $-77.0^\circ$  and a declination of  $0.5^\circ$ , approximately opposite to the present magnetic field. The block of reversed polarity is at a depth between 4 and 6 km on Profile 18 (Fig. 5.8) and between 4 and 8 km depth on Profile 24 (Fig. 5.13). The varying width and depth extension causes the different magnetic amplitudes, which can be observed from the southwest to the northeast. A better estimate of the geometry of these magnetic bodies could be derived by a 3D model with a higher lateral resolution.

### 5.3.1 The vanishing oceanic fracture zones

Oceanic spreading anomalies 24A and 24 B can be traced continuously through the survey area (Figs. 3.1, 3.2, 3.7, 5.14 & 5.15). The eastern side of the 24B anomaly is distorted by the magnetic anomalies originating from the lava flows (seaward dipping reflectors) that are actually an integrated part of the 24A and 24 B spreading anomalies. The western side of the 24 A-B anomalies are more undisturbed and therefore, most suitable for tracing these anomalies. Line drawing of the anomalies shows that they make a gentle convex, uninterrupted, bend to the west of the Røst Basin. Our reinterpretation of the oceanic spreading anomalies deviates significantly from earlier interpretations with reported offsets of up to 50 km (e.g. Hagevang et al. 1983, Blystad et al. 1995, Tsikalas et al. 2001, 2003, Olesen et al. 2002). The new data compilation shows that there are no significant offsets along any of the previously proposed zones. They were merely an artefact of wide profile spacing, poor navigation and poor levelling of the vintage aeromagnetic profiles. Brekke (2000) did also question the large offset along the Bivrost Fracture Zone.

Hagevang et al. (1983) did also interpret the Vøring fracture zone to explain an apparent offset of 24A and 24B anomalies on the outer Vøring Marginal High (to the southwest of our project area). This fracture zone was later named the Gleipne Fracture Zone by Blystad et al. (1995). Hagevang et al. (1983) interpreted a doubling of the 24A and 24B anomalies southwest of the Vøring fracture zone and an abandoned spreading ridge in the middle of the anomalies. From the existing aeromagnetic anomaly map of this area (Olesen et al. 1997a) we question the proposed doubling of spreading anomalies and recognise a need for modern aeromagnetic data on the Vøring Marginal High to resolve this problem.

## 5.4 Regional structures

### 5.4.1 Røst Basin – Flakstad high

The continent-ocean boundary (COB) along the Lofoten margin marks the western margin of the Røst Basin and is expressed as a pronounced gravity gradient running along a gentle arc-shaped curve (Figs. 3.3, 3.5 - 3.7, 5.14 & 5.15). Our COB has been adjusted compared with previous interpretations. Blystad et al. (1995) and Mjelde et al. (1992) interpreted a sharp bend in COB at 69°N, 10°E. This deflection deviates significantly from the course of the oceanic spreading anomalies to the northwest as well as the gravity gradient running along the COB further to the northeast and southwest. Our proposed new location for COB makes the distance to spreading anomaly 24B more even and coincides with the location of the observed gravity gradient. The gravity field is approximately 30 mGal lower inside the basin compared to the oceanic crust to the northwest. The depth to the basement is c. 9 km. The new aeromagnetic compilation corroborate the existence of a gap in the Vøring escarpment to the west of the Røst Basin as interpreted by Tsikalas et al. (2001). The missing escarpment may indicate that the basalt flows were deposited sub-aerially over the Røst Basin all the way to the palaeo-escarpment along the Utrøst Ridge. This interpretation is contrary to the conclusion by Berndt et al. (2001) who favoured a deep marine deposition but in support of the Tsikalas et al. (2001, 2002) interpretations.

The COB is displayed with a line (pale blue) on the interpretation maps (Figs. 3.7, 5.14, 5.15 and Map 7) although both gravity and aeromagnetic data (Figs. 3.1 - 3.6 and Maps 1 - 6) indicate a gradual 'oceanisation' of the continental crust across a transition zone between the two crustal types. Focused Euler solutions rarely occur along the interpreted COB, corroborating the inference that the boundary is a transition zone. Our new interpretation of the COB implies that transition from oceanic to continental crust is rather narrow to the west of the Røst Basin but widens to the northeast along the Lofoten margin where the gravity field is more complex. This is opposite to the interpretation by Tsikalas et al. (2002) who interpreted a narrowing of the COT from 50 km in the south to 30 km in the north (offshore Andøya).

The bulk of the magnetic rocks in the Røst Basin represents volcanics since the Euler depths are shallower than basement depths obtained from seismic data and gravity modelling. High frequency magnetic anomalies, representing the flow basalts, occurring as both negative and positive anomalies in a continuous zone from the western margin of the Hel Graben northeastwards to the eastern margin of the Røst Basin and up along the shelf edge to Andøya (Figs. 3.1 & 3.2). The depths to the igneous bodies and their spatial distribution have been studied using the Euler solutions applying a structural index of 1 and 0.5. Applying a

structural index of 1 yields the best result from the western areas and helps in locating edges of the intrusives and extrusives. The line 'eastern extent of Tertiary lava flows', or 'inner flows', (Blystad et al. 1995 and modified according to Tormod Henningsen, pers. comm. 2003) is marked in the maps (Figs. 3.1 & 3.2, Maps 1 & 2). The correlation between the eastern edge (violet line in the figure) and magnetic anomalies is, however, locally weak. We see that southeast of this line, the aeromagnetic anomalies are smoother than to the north of this line. This suggests that the high frequency anomalies may relate to intrusive and extrusive rocks within the sediments (see model across the Vøring Escarpment in Olesen & Skilbrei 1993), and that these generally occur to the northwest of this line. In general, one would expect Euler solutions to occur above edges of flows, strong topography, or where steps/abrupt changes in thickness of flows and intrusives occur. Semi-linear and curved features seen in well-focused Euler solution are interpreted as intrasedimentary magnetic sources. The location of focused Euler solutions marks structural features in the volcanic material (flows). These may relate to primary (formed during emplacement of the basalts) or secondary features (e.g. due to faulting, erosion, weathering, folding, subcrop).

Euler solutions align along the magnetic sea floor spreading anomalies. The linear focusing of the solutions and the depth estimates indicate sources within the upper part of the oceanic crust, as expected.

The occurrence of a pronounced positive gravity anomaly ( $68^{\circ}30'N, 10^{\circ}30'E$ ) of 30 mGal in the Røst Basin is puzzling. The anomaly may be interpreted in terms of 1) a basement high, 2) Late Cretaceous - Early Tertiary mafic intrusions within the sedimentary sequence, or 3) a dense (mafic) body within the basement. No high-velocity body was identified on OBS-line 4 by Mjelde et al. (1992) but the basement is approximately 1 km shallower in the eastern part of the basin compared to the 8 km deep western part. There is no magnetic anomaly coinciding with the gravity anomaly. Mafic intrusive rocks are usually (but not always) highly magnetic. Both the aeromagnetic data and the OBS-data therefore lend support to the interpretation of a deep-seated non-magnetic basement high at a depth of 6 km in the Røst Basin to the northwest of the Røst High. We apply the informal name Flakstad high for the structure. OBS-line 4 is located at the southwestern termination of the high and is consistent with basement located at 7 km depth in this part of the basin. The shape of the structural high and the interpreted depth of the Flakstad high are similar to the Sandflesa high further to the south. The latter has, however, been interpreted as a centre for voluminous mafic intrusions contributing to a gravity anomaly of 90 mGal. The Flakstad high consists of low-magnetic rocks, most likely representing Caledonian nappes or amphibolite-facies Precambrian gneisses.

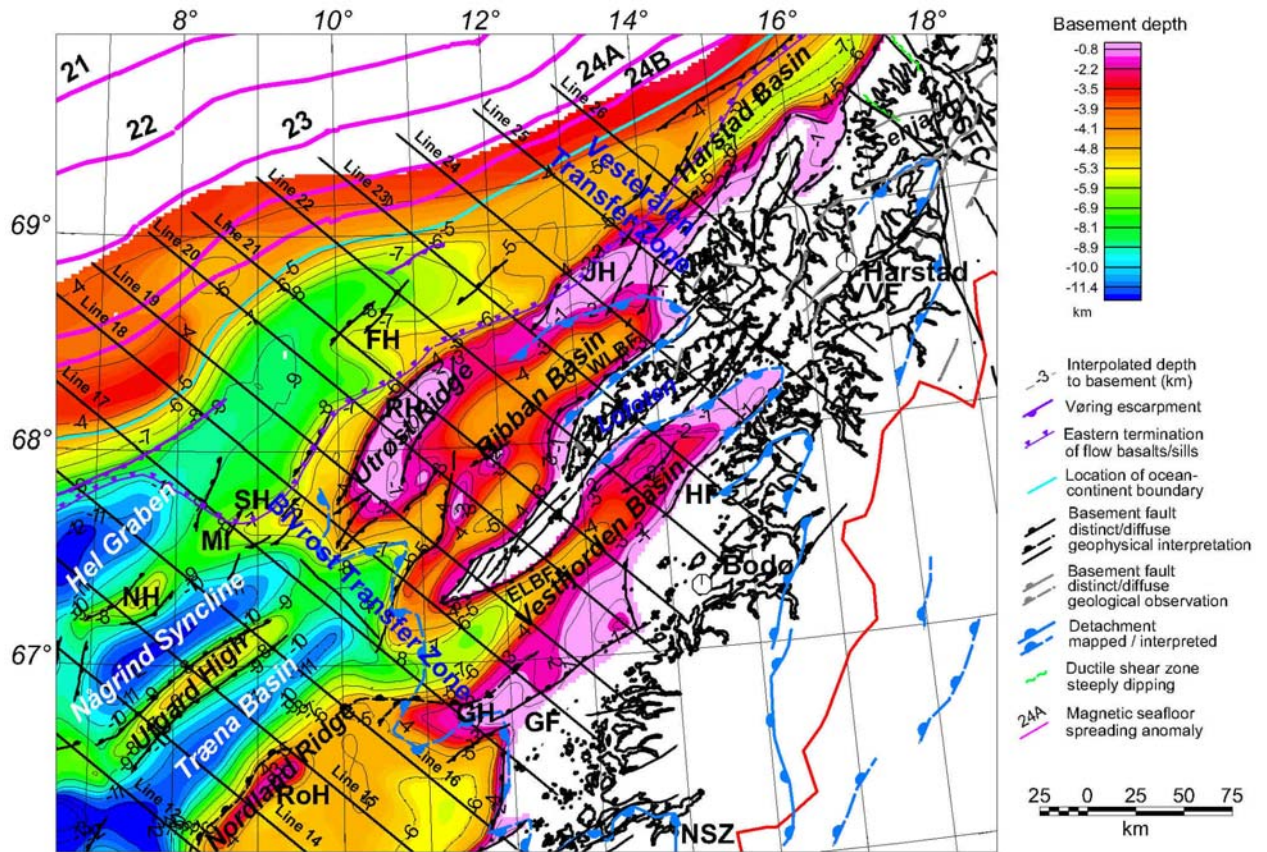


Figure 5.15 Regional basement structures within the Nordland area. The depth to basement surface represents depth to crystalline rocks. NSZ - Nesna shear zone, SSZ - Sagfjord shear zone; GF - Grønna fault, HF - Hamarøya fault; FH - Flakstad High; JH— Jennegga High; SH - Sandflesa High; RH - Røst High; NH - Nyk High; RoH – Rødøy High; GH – Grønøy High; VFZ - Vesterdjuvet Fault Zone; BSFC - Bothnian-Senja fault complex; VVF - Vestfjorden-Vanna fault complex; WLBF - Western Lofoten border fault; ELBF - Eastern Lofoten border fault; MC - Myken volcanic complex. The nomenclature is adapted from Andresen & Forshund (1987), Blystad et al. (1995), Løseth & Tveten (1996), Olesen et al. (1997b), Tsikalas et al. (2001) and Braathen et al. (2002).

Tsikalas et al. (2001) identified two windows in the lava flows to the southwest of the Røst High and to the west of the Jennegga High. Tilted sequences of seismic reflective bedrock were observed. We have not been able to recognize these windows in the new potential field data compilations. The lack of basalt flows inside the window would create a local negative gravity anomaly and a magnetic contact anomaly. These windows should have significant local effects on the gravity field if the thickness of the lava flow is several hundred metres. Converting the velocities of the volcano-sedimentary sequences (4400 and 5200 /s) to an average density of 2580 kg/m<sup>3</sup> (using the equation of Ludwig et al. 1970) provides a significant density contrast to the surrounding sedimentary rocks with a density of 2200-2400 kg/m<sup>3</sup>. The lack of magnetic anomalies along the border of the windows imply that flow basalts must be very thin or non-magnetic adjacent to the windows. This is not likely because the same flows

produce large amplitude anomalies at the termination to the east. The tilted seismic reflectors in these areas could be the effect of internal deformation within the Eocene volcano-sedimentary sequence rather than Mesozoic sediments below the flows. Alternatively, the rotated bedding that Tsikalas et al. (2001) interpreted to "protrude" from "lava windows" can relate to slump blocks that slid from the Utrøst Ridge into the Røst Basin during the deposition of the basalts. Fault scarp degradation, involving sliding of relatively large fault blocks from an exposed footwall block and onto the surface of the hangingwall block, is a well-known process in e.g. the northern North Sea (e.g. Underhill et al. 1997). The major westward deviation of the lava boundary to the west of the Jennegga High (Tsikalas et al. 2001) is a feature we find no evidence for in the aeromagnetic data.

Tsikalas et al. (2001) associated the observed volcanic build-up/mounds along the Lofoten margin with leakage zones at the eastern termination of the fracture zones. This mechanism is difficult to envisage since the fracture zones do not exist.

#### 5.4.2 Sandflesa High - Myken intrusive complex

The coinciding positive gravity and aeromagnetic anomaly located between the Utgard High and the Utrøst Ridge (Figs. 3.1 - 3.6) is caused by the Myken volcanic complex and Sandflesa high (Olesen et al. 2002). There is also a shallow Moho (22 km) in this area (Mjelde et al. 1998) contributing to one of the largest observed gravity anomalies (90 mGal) on the Mid-Norwegian continental margin. The magnetic anomaly is restricted to a smaller area than the gravity anomaly. Profile 17 (Fig. 5.7) crosses the Myken complex to the south of the Bivrost Lineament. The depth to the magnetic sources is approximately 3 km below the sea floor (Figs. 3.7 & 5.15). The complex has a dimension of 15 km by 40 km horizontally, and a depth extent of 9 km. We conclude that three models may explain the gravity and magnetic anomalies: (a) mafic igneous intrusions, (b) a basement high or (c) a thick sequence of flow basalt rocks. Interpretation (a) is favoured because Mjelde et al. (1998) have reported intermediate seismic velocities (4-5 km/s) at a depth of 7 km in this area. Sedimentary rocks must therefore occur below the high-density body. A shallow basement high is not a viable model although basement rocks could form a positive structure at larger depth in this area, as indicated in Fig. 5.7. The large size of the body points to an intrusive complex rather than a thick pile of extrusives. We envisage a complex mixture of volcanic and sedimentary rocks within this magmatic centre. The 3D model is simplified to a simple, box-shaped body (Fig. 5.7). Berndt et al. (2001) have interpreted a gently-dipping, strong seismic reflection in terms of a tuff sheet in the Myken area. An alternative interpretation is an erosional surface in sub-aerial volcanics. The Hel Graben to the west has earlier been interpreted to be a centre of igneous activity on the basis

of seismic velocities (Mjelde et al. 1998, Berndt et al. 2000). Our interpretation suggests that a basement high (Sandflesa High) is situated below the Myken intrusive complex and a sedimentary succession. This is also consistent with earlier interpretation by Olesen et al. (1997b) and Mjelde et al. (1998). Some of the deepest Euler depths (7km-8km) may represent the top of the basement. The shallowest depths must represent intrasedimentary volcanic rocks.

The age of the intrusions is uncertain, but a Palaeocene age is likely considering the mid to Late Paleocene age of magmatism in the North Atlantic Volcanic Province (e.g. Saunders et al., 1997), and particularly the Late Paleocene age of the lower series drilled in DSDP 642 on the Vøring Marginal High (Sinton et al. 1998). The Myken volcanic complex may resemble seamounts or 'hot points' occurring as intrusive (dolerite/gabbro/peridotite) complexes in the Red Sea (Bonatti & Seyler 1987, Cochran & Martinez 1988). Lundin & Doré (1997) have interpreted similar seamounts in the central Møre Basin, and seamounts are well-known in the Rockall Trough and the Faeroe-Shetland Basin. The latter intrusive complexes are mostly of Palaeocene age (Stoker et al. 1993). The gradient of the gravity field is highest on the eastern flank of the Sandflesa anomaly indicating a boundary fault to the east (Figs. 3.3 - 3.6 & 5.7). The resolution of the 3D density model must be improved to provide more detailed results on the Myken complex - Sandflesa high area. The Myken Volcanic Complex occurs at the seawards projection of the Bivrost transfer zone (Olesen et al. 2002). To the northwest of the Myken volcanic complex a broad northwest-oriented zone occurs where the magnetic field is more erratic. This is seen in both the magnetic total field and in the residual map. The Euler depth solutions point towards both relatively shallow depths around 3 km, and some relatively deep magnetic contacts (> 5 km) that may represent intrusives. In this area, three main orientation are expressed by the Euler solution: NW-SE, NE-SW, and N-S. These may represent faults or weakness zones along which intrusives have ascended (see also Brekke, 2000). These trends are also observed in the Lofoten area, suggesting that the basement underneath the Røst basin has a structural grain comparable to that of the Lofoten area. Some of the Euler solutions line up along curvilinear segments. These may represent edges of flows. In the residual map, as well as in the Euler depths, E-W to ENE-WSW features are observed that may represent deep basin segmentation or volcanic transition zones.

### 5.4.3 Utgard High

The Utgard High is a 140 km long NE-trending basement high with steep flanks on both sides, most likely consisting of one or more steep normal faults. The basement high produces characteristic gravity and magnetic anomalies that produce quite consistent depth estimates. The Euler depths are shallowest in the central part of the high and gradually become deeper toward the margins, indicating one or more basement blocks along the flanks of the high. The depth to the shallowest part of the basement high is approximately 6.5 km. The depth increases gradually to the northeast and southwest along the crest of the high to depths of approximately 8 km. The basement of the Træna Basin and Någrind Syncline to the southeast and northwest are located at a depth of minimum 11 and 12 km, respectively, revealing a structural relief in the order of 4-6 km. The northwestern flank is overlain by mafic sills and is consequently difficult to identify on seismic data. It is notably the gravity data that reveal the abrupt basement drop along the outer part of the Utgard High. The long wavelength component of the gravity anomaly is caused by a shallow Moho, located at a depth of 18 - 19 km below the basement high. The deep structure of the Utgard High resembles to a large degree the Lofoten Ridge, where steep normal faults bound both sides and where the Moho reveals a prominent shallow bulge underneath. These geometries can be explained in terms opposing halfgrabens, with overlapping zones of uniform crustal thinning at depth (Nick Kuszniir, pers comm. 2003).

From the Utgard High (Figs. 5.16 - 5.17), we tested the Euler depth solutions against forward model solutions and the Naudy depths using Modelvision software (Figs. 5.18 & 5.19). Initially a profile was selected to test the parameters used in the modelling procedure. When depth solutions were found satisfactory, these parameters were applied to all the other required profiles across the Utgard High. Specifically, the susceptibility values were compared to those of rock samples onshore (Olesen et al. 2002). The width of the causative bodies was estimated directly, and by an inversion process described by Encom (2003). Finally, depth to the top and the bottom of the source was inverted upon. In order to use a simple geometry, the bottom was set to 18-20 km, close to the Curie point isotherm of the area (see above). The depth estimates were used in the contouring of the basement surface. The results closely agree with earlier results reported by Olesen et al. (2002). A forward model along Profile 80 is shown in Fig. 5.18.



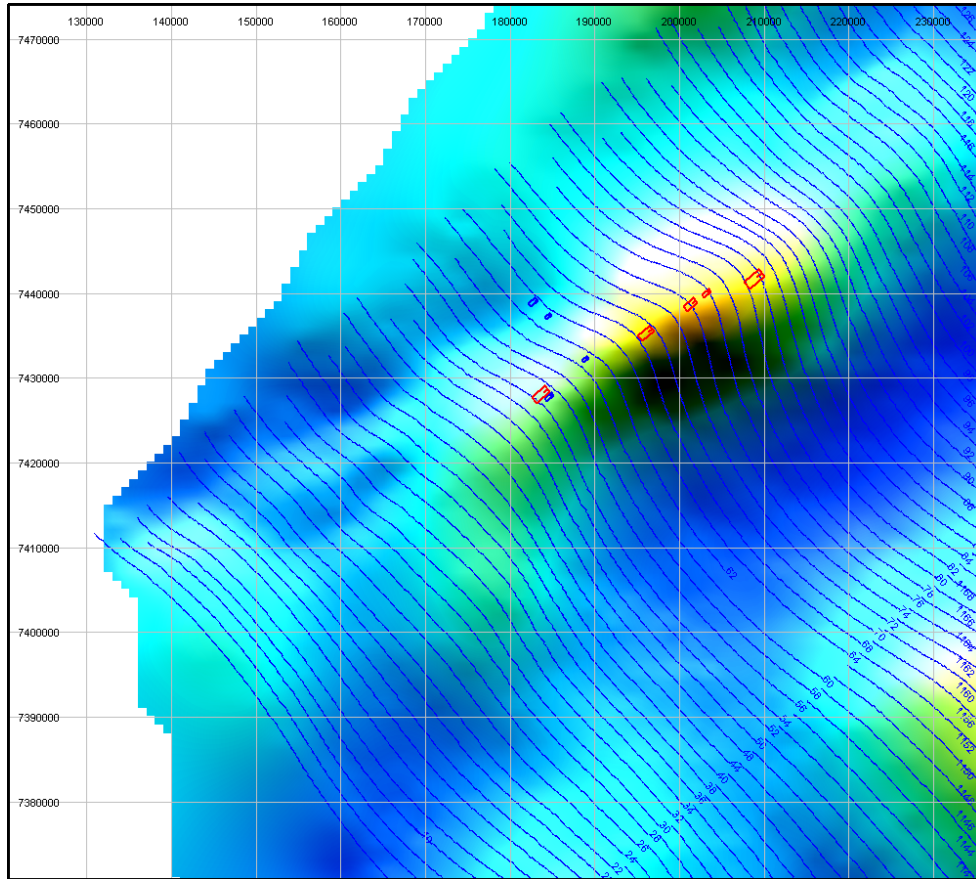


*Figure 5.16 Shaded relief version of magnetic data of the Utgard High and surrounding areas and stacked magnetic profiles. Line numbers are shown. Rectangles represent location of Naudy depth-solutions. See text for explanation, and next figure. Note that coordinates are in UTM zone 33.*

Two sills were penetrated by well 6607/2-1 on the Utgard High at depth intervals of 3792-3886 m and 4640-4697 m. There is apparently no magnetic signal from these sills. This may be caused by low susceptibility and remanence, thin sills and/or large depth to the intrusions. The long wavelength signal originating from the basement will not mask anomalies from the intrusive rocks. Although there is some low-amplitude noise in the original profile data, we believe that it would not mask coherent signals from the sills.

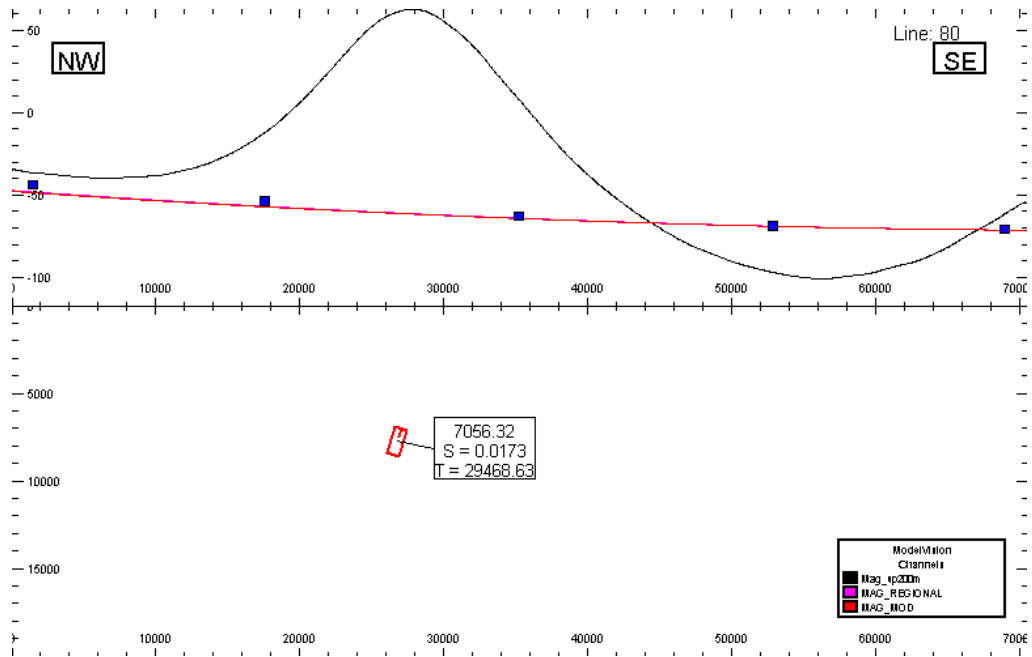


Figure 5.17 Example of Naudy depth solution along Profile 80, crossing the Utgard High. Numbers inside the rectangle refer to depth to the top (upper number), Susceptibility ( $S$ ), and thickness of block ( $T$ ), representing the basement block of the Utgard High. Similar depth solutions were obtained also from other lines crossing the Utgard High. The solutions have been plotted on the maps, together with Euler- and autocorrelation-estimates (Figs. 3.1- 3.7, Maps 1 - 7).

To the southwest and west of the Utgard High, a negative anomaly occurs that may be associated with remanently magnetised dolerite sills. In Fig. 5.18 magnetic forward modelling is shown that incorporates a ca. 500 m thick dolerite body in the middle of the Lower Cretaceous section. It may represent a single body or several sills. This interpretation is not conclusive as such a model depends on the interpreted regional field (zero level) and the dip of the 'basement bodies'. An alternative interpretation is shown in Fig. 5.19, without dolerites. However, the fit is poorer to the negative anomaly to the west of the Utgard High. Thus, we suggest that deeply buried dolerites exist between the Nyk High and the Utgard High. This may be somewhat similar to the model to the west of the Nyk High (see model in Lundin et al. in prep.). In the seismic sections, high amplitude reflectors occur near the basement on the western side of the Utgard High (P. Midbøe, pers. comm. 2003).

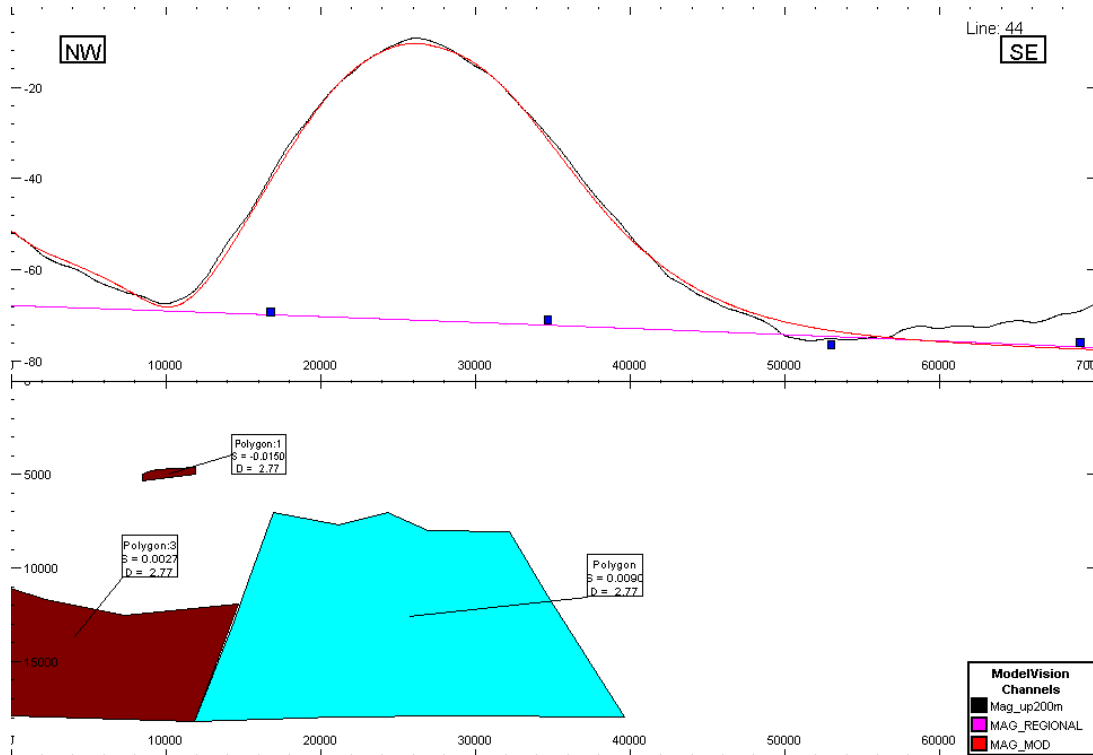


Figure 5.18 Magnetic forward model along Profile 44. The model shows that the main anomaly above the Utgard High can be caused by the basement block. The rather sharp negative anomaly on the western side of the high (eastern part of the Någrind Syncline) is explained by remanent magnetisation of dolerite intrusions that occur at a depth of around 5000 m in the syncline. Applied magnetic susceptibility of the basement is 0.01 (blue 'basement body'), 0.0027 (brown basement body), and 0.01 (brown basement body, left in profile. The dolerite has a negative susceptibility of  $-0.027$  (units in SI).

In the forward model of the Utgard High, we aimed at keeping the body as simple as possible. The magnetisation values are relatively high, not much lower than used in the 3D models (see above). At depths of  $> 5 - 6$  km, details of the basement complex cannot be modelled. We have assumed some smooth topography of the top basement surface on the basement high. The basement high has a steep slope towards the basins on either side. It may represent eroded rift flank relief. An alternative model is to assume that the western slope of the basement high consists of relatively narrow fault blocks, occurring successively at deeper positions basinwards (Olesen & Myklebust 1989).

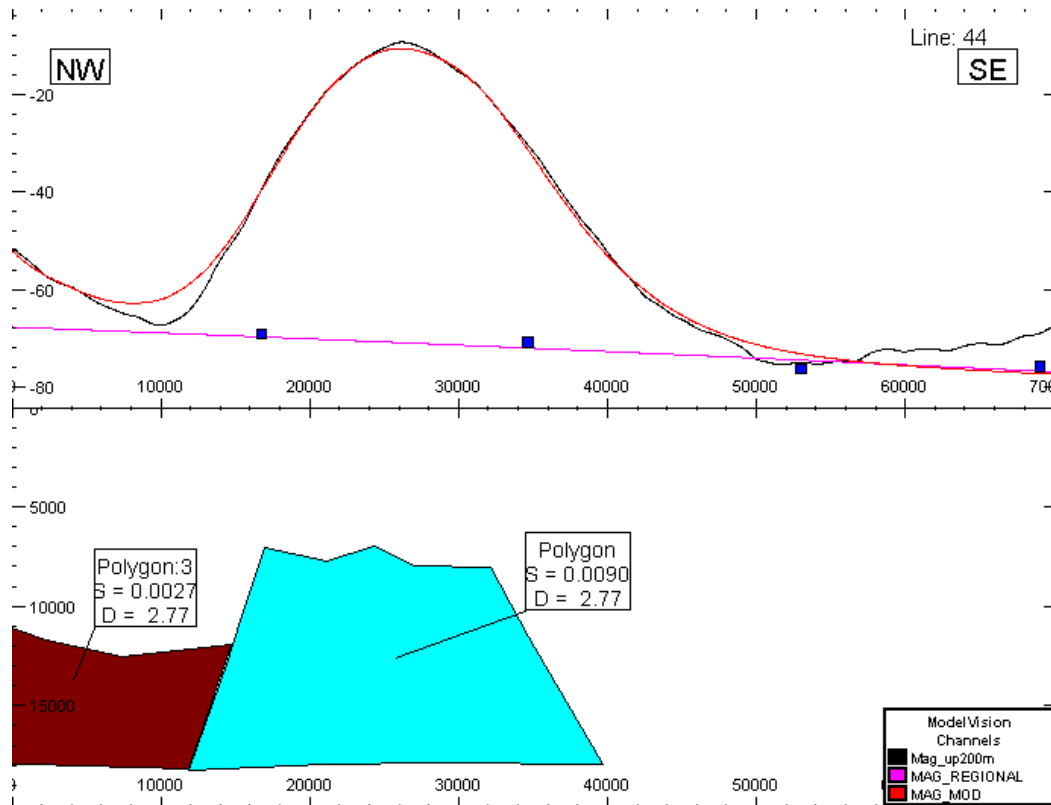


Figure 5.19 Alternative forward model along Profile 44, without dolerite intrusion in the Nâgrind Syncline. Compare with Fig. 5.18. Note that a poorer fit between observed and modelled magnetic curve is achieved. See text for explanation.

The shelf edge at c. 300 m water depth produces a low-amplitude ( $< 10\text{nT}$ ), high-frequency magnetic anomaly. This edge constitutes a low magnetised body (the shelf) located next to the non-magnetic deep ocean. Despite the low magnetic contrast, it is sufficient to produce an anomaly because of the large volume involved (Skilbrei & Kihle 1999). This anomaly partly coincides with the anomaly from the easternmost termination of the flow-basalts. Previous interpretations have not distinguished between these two anomalies (Olesen & Myklebust 1989, Olesen & Torsvik 1993, Tsikalas et al. 2001, 2002).

The shallow depth estimates along the Nyk High to the southwest show that the corresponding magnetic anomaly is caused by the termination of reversed magnetised sills towards the structural high rather than magnetic basement rocks below.

#### 5.4.4 Utrøst Ridge - Ribban Basin

The Ribban Basin area is characterised by large depths to the magnetic basement. The largest depths, up to 10 km, correspond to the Skomvær and Havbåen Subbasins within the Ribban Basin. Modelling of gravity data give much shallower depths (up to 5 km). This discrepancy is interpreted to be caused by downfaulted low-magnetic Caledonian nappes or low-magnetic amphibolite-facies gneisses. Previous potential field studies in the areas have resulted in similar conclusions (Åm 1975, Olesen *et al.* 1997b). The occurrence of low-magnetic basement is illustrated on the interpretation profiles 18 – 22, Figs. 5.8 – 5.12). The Skomvær Basin is a half-graben bound by a steep fault towards the Lofoten Islands. A shallow basement ridge at 1-3 km depth between the Røst High and the Skomvær Subbasin corresponds with the Marmæle Spur. However, large depths to basement (c. 4 km, Figs. 3.7 & 5.15) are obtained from both gravity and magnetic data to the north of the Marmæle Spur, which are significantly different from the depths interpreted from multichannel seismics, indicating that there may be an approximately 2 km thick sequence of low-density sediments below the base-Cretaceous in this area. The quality of the multichannel reflection seismic data is poor in this particular area due to pronounced seafloor multiples.

Some of the depth estimates along the Utrøst Ridge represent depth to magnetic sources within the basement, i.e. below the basement surface. The occurrence of low-magnetic basement is also evident from the modelling of both Profile 19 and 20 (Figs. 5.9 & 5.10). Rotated fault-blocks have been interpreted on multichannel seismic data to the west of the large-scale faults along the seaward boundary of the Utrøst Ridge. These blocks are located immediately to the north of the Sandflesa high.

#### 5.4.5 Vestfjorden Basin

The southern part of the Vestfjorden Basin is a 7 - 8 km deep half graben defined by the east-dipping Eastern Lofoten border fault against the Lofoten Ridge, a geometry also shown by Brekke & Riis (1987). The northern part of the Vestfjorden Basin, however, is a shallower (approximately 2 km deep) half graben with the boundary fault, Hamarøya fault, along the eastern margin of the basin (Olesen *et al.* 1997b, 2002). The Mosken transfer zone is separating the areas with opposing fault throw. From the aeromagnetic maps we interpret the western margin in the Lødingen area to consist of several rotated fault blocks extending from Austvågøya and Hinnøya into the Vestfjorden Basin. Raftsundet and Øksfjorden have very conspicuous topographic and bathymetric expressions and coincide with negative magnetic anomalies that are located between the rotated, magnetic fault blocks. These fjords and sounds most likely contain the fault zones separating the rotated fault blocks.

#### 5.4.6 Harstad Basin

Uplift of the Vesterålen area is more dome-like in character compared with the sharp horst structure of the Lofoten Islands. The offshore basement-faults are also less distinct and the vertical offsets along them are smaller. However, the base of the Harstad Basin is at more than 7 km depth, west of Andøya. This depth has been interpreted from gravity data (Olesen *et al.* 1997b). All the depth estimates from the aeromagnetic interpretation are shallower, which is not surprising since they most likely represent depth to magnetic magmatic rocks. The magnetic anomalies at the eastern margin of the basin are continuous with structures in the Vesterålen islands and most likely reflect rotated blocks within the basement. The NE-SW trending high frequency anomalies in this area represent volcanic rocks. The easternmost anomalies occur along a zone coinciding with the shelf edge and most likely represent the easternmost limit of the flow-basalts. The interpreted depths to these anomalies are in the order of 0.5 - 2.0 km below sea level. Tsikalas *et al.* (2002) have not distinguished between the magnetic effect from the lava flows and the magnetic basement when tracing the eastern lava front.

## 6 CONCLUSIONS

1. The opening of the studied part of the Norwegian-Greenland Sea (from the central Vøring Basin to and including the Harstad Basin) occurred along a stable continental margin without offsets of oceanic spreading anomalies. This conclusion contrasts with previous interpretations of the magnetic oceanic spreading anomalies, and hence is contrary to previous interpretations for the opening phase of this area. We also question the previously interpreted fracture zones to the southwest on the Vøring Marginal High. They may also be non-existent. A new location of the continent-ocean boundary (COB) has been defined from the combined datasets. The distance to the ocean spreading anomaly 24 B is quite constant through the area. This also differs from prior interpretations of the area.

2. The structural setting of the Utgard High bears great resemblance to the Lofoten Ridge with large scale normal faults on either side and a shallow Moho caused by overlapping zones of uniform crustal thinning at depth.

3. The western boundary of the Utrøst Ridge is bounded by large faults with down to the northwest. Two basement highs, Sandflesa and Flakstad, occur at a depth of approximately 6 km to the southwest and west, respectively, of the Utrøst Ridge.

4. The Helgeland Nappe Complex has been downfaulted along the offshore extension of the Nesna shear zone. This interpretation is supported by the correspondence between the depth extent of the low-magnetic nappes on land and the thickness of the offshore low-magnetic basement (calculated as the difference between the offshore magnetic depth estimates and the depths obtained from gravity and seismic interpretations). The Sagfjord shear zone further north may analogously be extended below the low-magnetic amphibolite-facies gneisses beneath the Vestfjorden and Ribban basins.

5. The Bivrost, Vesterålen and Lenvik transfer zones define the regional segmentation of the Lofoten margin. The local Mosken and Melbu transfer zones are also located where shifts in polarity occur along faults and separate individual rotated fault blocks. This is most noticeable in the Ribban and Vestfjorden Basins but can also be observed further to the northeast along the Vestfjorden-Vanna fault complex. The Vesterålen transfer zone separates the Røst, Ribban and Vestfjorden basins in the south from the Harstad Basin in the north. Changes in Moho depths occur across the Bivrost and Vesterålen transfer zones indicating that these structures are continuous through the whole crust. The location of the transfer zones is not spatially connected to younger oceanic fracture zones as previously interpreted.

6. The combined interpretation of depth to basement reveals basin depths of 5 km in the Ribban Basin offshore Lofoten and 9 km in the Røst Basin. Greater depths to magnetic basement occur

locally, and are interpreted to represent down-faulted Caledonian nappes, Devonian sediments, or low-magnetic (amphibolite facies) Precambrian rocks.

7. A substantial excess of mass must occur in the crust to cause the observed large gravity anomaly (90 mGal) in the Sandflesa area. When taking into account existing seismic information, we conclude that the gravity and magnetic anomalies are most likely caused by large mafic intrusions in both the basement and the overlying sediments. There is most likely a complex mixture of volcanics and sediments within this volcanic centre.

8. Basement depth estimates from gravity and magnetic data to the east of the Utrøst Ridge and north of the Marmæle Spur show that there may exist an approximately 2 km thick sequence of low-density sediments below the base-Cretaceous unconformity in this area.

9. The closer line spacing of the RAS-03 aeromagnetic profiles compared to the old NGU-73 and NRL-73 surveys has provided a more detailed image of the magnetic sources in the Røst Basin area. Our work shows that the combined approach from interpretation of seismic data (both reflection and refraction), aeromagnetic and gravity data yields the best solutions. Relying on only one data-type provides less reliable results.



## **7 RECOMMENDATIONS FOR FURTHER WORK**

1. We propose to make a new aeromagnetic data compilation of the area within the two remaining months of the Ra 3 project. The SPT-93 grid included in the aeromagnetic compilation is smoothed. This is also evident from the aeromagnetic maps (Figs. 3.1 - 3.2) where the high-frequency part of this data set is quite subdued. No profile recordings were included in the archive tape produced by Simon Petroleum Technology for the SPT-93 project. Fugro Airborne Surveys (FAS) has acquired both companies Simon Petroleum Technology (SPT) and World Geoscience. The latter company (based in Perth, Australia) carried out the data acquisition of the SPT-93 survey. We ordered a new archive tape (including profile recordings) from FAS in Australia but did unfortunately not receive the new archive tape until late in the project period. BP acquired the eastern part of the VGVB-94 survey after the Ra 3 data compilation was finished. We do therefore recommend to include a new un-smoothed grid of the SPT -93 data as well as the VGVB-94 and VBAME-00 datasets in a new data compilation.

2. We have constructed a regional 3D model of the Nordland area. We suggest carrying out a more detailed 3D model for the Utgard-Myken-Utrøst area during the last phase of the project.

3. The significant improvements in delineating the regional tectonic setting along the Lofoten continental margin, and especially in locating the magnetic spreading anomalies, show that the new aeromagnetic survey in the Røst Basin was warranted. Considering these results one may question other proposed fracture zones in the oceanic crust, particularly off NE Greenland where data are poor quality and comparatively old. The coverage is especially poor on the Møre and Vøring marginal highs and along the western margin of the north and central Barents Sea. The aeromagnetic data on shelf areas of the central North Sea and the southeastern Barents Sea are acquired in early 1970s using Decca navigation and should also be replaced by modern high-resolution data. Pre-1980 seismic data are also today regarded as obsolete and are very seldom used for detailed interpretations. Based on the Ra 3 results we suspect that the same problems apply to the pre-1980 aeromagnetic surveys.

## **8 ACKNOWLEDGEMENTS**

BP Norge, Norsk Hydro, Statoil, NPD and NGU financed the Røst Aeromagnetics 2003 Project (Ra 3). Jan Nordås (Norsk Hydro), Tormod Henningsen (Statoil), Morten Sand (NPD) and Evan Kåre Hansen (BP Norge) gave advice during the project period. John Dehls, NGU provided bathymetric data. We express our thanks to these companies, institutions and persons.

## 9 REFERENCES

- Andersen, O.B. & Knudsen, P. 1998: Gravity anomalies derived from the ERS-1 satellite altimetry. Kort og Matrikelstyrelsen, DK-2400 Copenhagen NV, Denmark (www.kms.dk).
- Andresen, A. & Forslund, T. 1987: Post-Caledonian brittle faults in Troms: geometry, age and tectonic significance. *The Caledonian and related geology of Scandinavia* (Cardiff, 22-23 Sept., 1989) (Conf. abstr.).
- Berndt, C., Skogly, O.P., Planke, S., Eldholm, O. & Mjelde, R. 2000: High-velocity breakup-related sills in the Vøring Basin, off Norway. *Journal of Geophysical Research* 105, 28.443-28.454.
- Berndt, C., Planke, S., Alvestad, E., Tsikalas, F. & Rasmussen, T. 2001: Seismic volcanostratigraphy of the Norwegian Margin: constraints on tectonomagmatic breakup processes. *Journ. Geol. Soc. London* 158, 413-426.
- Blakely, R.J. & Simpson, R.W. 1986: Approximating edges of source bodies from magnetic or gravity anomalies. *Geophysics* 51, 1494-1498.
- Blystad, P., Brekke, H., Færseth, R.B., Larsen, B.T., Skogseid, J. & Tørudbakken, B. 1995: Structural elements of the Norwegian continental shelf, Part II. The Norwegian Sea Region. *Nor. Petr. Dir. Bull.* 8, 45 pp.
- Bonatti, E. & Seyler, M. 1987: Crustal underplating and evolution in the Red Sea Rift: uplifted gabbro/gneiss complexes on Zabargad and Brothers islands. *Journ. Geophys. Research* 92, 12.803-12.821.
- Breivik, A.B., Verhoef, J. and Faleide, J.I. 1999: Effects of thermal contrasts on gravity modeling at passive margins: results from the western Barents Sea. *JGR*, 104, 15293-15311.
- Brekke, H. 2000: The tectonic evolution of the Norwegian Sea continental margin with emphasis on the Vøring and Møre basins. In Nøttvedt, A. et al. (eds.) *Dynamics of the Norwegian Margin*. Geological Society of London, Special Publication 167, 327-378.
- Brekke, H. & Riis, F. 1987: Tectonics and basin evolution of the Norwegian shelf between 62° and 72°N. *Nor. Geol. Tidsskr.* 67, 295-322.
- Breunig, M., Cremers, A.B., Götze, H.-J., Schmidt, S., Seidemann, R., Shumilov, S. and Siehl, A., 2000: Geological Mapping based on 3D models using an Interoperable GIS. *Geo-Information-Systems. Journal for Spatial Information and Decision Making* 13, 12-18.
- Braathen, A., Nordgulen, Ø., Osmundsen, P.T., Andersen, T.B., Solli, A. & Roberts, D. 2000: Devonian, orogen-parallel, opposed extension in the Central Norwegian Caledonides. *Geology* 28, 615-618.
- Braathen, A., Osmundsen, P.T., Nordgulen, Ø. & Roberts, D. 2002: Orogen-parallel, extensional denudation of the Caledonides in North Norway. *Norsk Geologisk Tidsskrift* 82. 225-241.
- Cande, S.C. & Kent, D.V. 1995: Revised calibration of the geomagnetic polarity timescale for the Late Cretaceous and Cenozoic. *Journ. Geophys. Res.* 100, 6093-6095.

- Cochran, J.R. & Martinez, F. 1988: Evidence from the northern Red Sea on the transition from continental to oceanic rifting. *Tectonophysics* 153, 25-53.
- Colletta, B., Le Quellec, Letouzey, P. & Moretti, I. 1988: Longitudinal evolution of the Suez rift structure (Egypt). In X. Le Pichon & J.R. Cochran (eds.), The Gulf of Suez and Red Sea Rifting. *Tectonophysics* 153, 221-233.
- Eide, E.A., Osmundsen, P.T., Meyer, G.B., Kendrick, M.A. & Corfu, F. 2002: The Nesna Shear Zone, north-central Norway: an  $^{40}\text{Ar}/^{39}\text{Ar}$  record of Early Devonian – Early Carboniferous ductile extension and unroofing. *Norsk Geologisk Tidsskrift* 82, 317-339.
- Eldholm, O., Sundvor, E. & Myhre, A. 1979: Continental margin off Lofoten-Vesterålen, Northern Norway. *Marine Geophys. Res.* 4, 3-35.
- Eldholm, O., Thiede, J. & Taylor, E. et al. (Eds.) 1987: Proc. ODP, Initial Reports 104, College Station, TX (Ocean Drilling Program).
- Eldholm, O., Thiede, J. & Taylor, E. and shipboard scientific party 1987: Summary and preliminary conclusions, ODP leg 104. In Eldholm, O., Thiede, J. & Taylor, E. et al. Proc. ODP, Initial Reports 104, 751-771.
- Eldholm, O., Tsikalas, F. & Faleide, J.I. 2002: The continental margin off Norway 62-75°N: Palaeogene tectono-magmatic segmentation and sedimentation. In: D. Jolley & B. Bell (eds.). The North Atlantic Igneous Province: stratigraphy, tectonics, volcanic and magmatic processes. *Geol. Soc. London Spec. Publ.* 197, 39-68.
- Encom 2003: Automag (Modelvision Pro option v5.0), Online Reference Manual pp. 117-153.
- Fichler, C., Rundhovde, E., Olesen, O., Sæther, B.M., Rueslåtten, H., Lundin, E. and Doré, A.G., 1999. Regional tectonic interpretation of image enhanced gravity and magnetic data covering the Mid-Norwegian shelf and adjacent mainland. *Tectonophysics*, 306, 183-197.
- Gaal, G. & Gorbatshev, R. 1987: An outline of the Precambrian evolution of the Baltic Shield. *Precambrian Research* 35, 15-52.
- Gabrielsen, R.H., Færseth, R.B., Jensen, L.N., Kalheim, J.E. & Riis, F. 1990: Structural elements of the Norwegian continental shelf, Part I: The Barents Sea Region. *Norwegian Petroleum Directorate Bulletin* 6, 33 pp.
- Geosoft 2000a: Geosoft GridKnit, Grid stitching tool for OASIS montaj, Tutorial and user guide, Geosoft Incorporated, 28 pp.
- Geosoft 2000b: MAGMAP (2D-FFT), 2-D frequency domain processing of potential field data, Geosoft Incorporated, 67 pp.
- Geosoft 2001: OASIS Montaj v 5.1, The core software platform for working with large volume spatial data. Data Processing System for Earth Sciences Applications. Users manual, Geosoft Incorporated, 228 pp.
- Geosoft 2003: 3-D Euler 3D deconvolution (v5.1.5). Processing, Analysis and Visualization System for 3D Inversion of Potential Field Data, Tutorial and users guide. Geosoft Incorporated, 64 pp.
- Götze, H.-J. and Lahmeyer, B., 1988. Application of three-dimensional interactive modeling

in gravity and magnetics. *Geophysics*, 53(8): 1096-1108.

- Hagevang, T., Eldholm, O. & Aalstad, I. 1983: Pre-23 magnetic anomalies between Jan Mayen and Greenland-Senja Fracture Zones in the Norwegian Sea. *Marine Geophysical Researches* 5, 345-363.
- Hames, W.E. & Andresen, A. 1996: Timing of Paleozoic orogeny and extension in the continental shelf of north-central Norway as indicated by laser  $^{40}\text{Ar}/^{39}\text{Ar}$  muscovite dating. *Geology* 24, 1005-1008.
- Hartz, E.H., Eide, E.A., Andresen, A., Midbøe, P., Hodges, K.V. & Kristiansen, S.N. 2002:  $^{40}\text{Ar}/^{39}\text{Ar}$  geochronology and structural analysis: Basin evolution and detrital feedback mechanisms, Hold With Hope region, East Greenland. *Norsk Geologisk Tidsskrift* 82, 341-358.
- Heiskanen, W.A. & Moritz, H. 1967: Physical Geodesy. *W.H. Freeman, San Fransisco*. 364 pp.
- Henkel, H. 1991: Magnetic crustal structures in Northern Fennoscandia. In: P. Wasilewski & P. Hood (Eds.). Magnetic anomalies — land and sea. *Tectonophysics* 192, 57-79.
- Henkel, H. & Guzmán, M. 1977: Magnetic features of fracture zones. *Geoexploration* 15, 173-181.
- Henkel, H. & Eriksson, L. 1987: Regional aeromagnetic and gravity studies in Scandinavia. *Precambrian Research* 35, 169-180.
- Hunt, C., Moskowitz, B.M., Banerje, S.K., 1995: Magnetic properties of rocks and minerals. In: Rock Physics and Phase Relations. A Handbook of Physical Constraints. AGU Reference Shelf 3, pp. 189-204.
- Kent, D.V. & Opdyke, N.D. 1978: Paleomagnetism and magnetic properties of igneous rock samples – Leg 38. In Talwani, Udintsev *et al.* (Eds.) Initial reports of the Deep Sea Drilling Project, Supplements to Vol. 38, 39, 40 and 41. *Govt. Printing Office, Washington, D.C.*, 3-8.
- Kinck, J.J., Husebye, E.S. and Larsson, F.R., 1993: The Moho depth distribution in Fennoscandia and the regional tectonic evolution from Archean to Permian times, *Precambrian Research*, 64, 23-51.
- Ludwig, J.W., Nafe, J.E. and Drake, C.L. 1970: Seismic refraction. In: Maxwell., A. (ed.): *The sea*, Vo.4, Wiley, New York.
- Lund, C-E. 1979: Crustal structure along the Blue Road Profile in northern Scandinavia. *Geologiska Föreningens i Stockholm Förhandlingar* 101, 191-204.
- Lundin, E.R., Rønning, K., Doré, A.G. & Olesen O. 2002: Hel Graben, Vøring Basin, Norway – a possible major cauldron? Abstract, 25<sup>th</sup> Nordic Geological Winter Meeting, January 6<sup>th</sup> - 9<sup>th</sup>, 2002, Reykjavik.
- Lundin, E.R., Doré, A.G. 1997: A tectonic modell for the Norwegian passive margin with implications for the NE Atlantic: Early Cretaceous to break-up. *Journ. Geol. Soc. London* 1584, 545-550.
- Løseth, H. & Tveten, E., 1996: Post-Caledonian structural evolution of the Lofoten and Vesterålen offshore and onshore areas. *Norsk Geologisk Tidsskrift* 76, 215-230.
- Mathisen, O. 1976: A method for Bouguer reduction with rapid calculation of terrain corrections. *Geographical Survey of Norway geodetic publications* 18, 40 pp.

- Mauring, E., Smethurst, M.A. & Kihle, O. 1999: Vestfjorden Aeromagnetic Survey 1998. Acquisition and processing report. *NGU Report 99.001*, 23 pp.
- Mauring, E., Beard, L.P., Kihle, O. & Smethurst, M.A. 2002: A comparison of aeromagnetic levelling techniques with an introduction to median levelling. *Geophysical Prospecting* 50, 43-54.
- Mauring, E., Mogaard, J.O. & Olesen, O. 2003: Røst Basin Aeromagnetic Survey 2003 (RAS-03). Ra 3 aeromagnetic compilation. Data acquisition and processing report. NGU Report 2003.070, 20 pp.
- Mjelde, R., Sellevoll, M.A., Shimamura, H., Iwasaki, T. and Kanazawa, T. 1992: A crustal study off Lofoten, N.Norway, by use of 3-component ocean bottom seismographs. *Tectonophysics* 212, 269-288.
- Mjelde, R., Sellevoll, M.A., Shimamura, H., Iwasaki, T. and Kanazawa, T. 1993: Crustal structure beneath Lofoten, N.Norway, from vertical incidence and wide-angle seismic data. *Geophysical Journ. Int.* 114, 116-126.
- Mjelde, R., Kodaira, S., Shimamura, H., Kanazawa, T. Shiobara, H., Berg, E.W. & Riise, O. 1997: Crustal structure of the central part of the Vøring Basin, mid-Norway margin, from ocean bottom seismographs. *Tectonophysics* 277, 235-257.
- Mjelde, R., Digranes, P., Shimamura, H., Shiobara, H., Kodaira, S., Brekke, H., Egebjerg, T., Sørenes, N. & Thorbjørnsen, S. 1998: Crustal structure of the northern part of the Vøring Basin, mid-Norway margin, from wide-angle seismic and gravity data. *Tectonophysics* 293, 175-205.
- Mokhtari, M. & Pegrum, R.M. 1992: Structure and evolution of the Lofoten continental margin, offshore Norway. *Nor. Geol. Tidsskr.* 72, 339-355.
- Murthy, I.V.R. & Rao, S.J. 1989: Short note: A Fortran 77 program for inverting gravity anomalies of two-dimensional basement structures. *Computing & Geosciences* 15, 1149-1156.
- Mørk, M.B. & Olesen, O. 1995: Magnetic susceptibility of sedimentary rocks from shallow cores off Mid Norway and crystalline rocks from the adjacent onland areas. NAS-94 Interpretation Report, Part II: Petrophysical data. *NGU Report 95.039*, 68 pp
- Mørk M.B.E., McEnroe, S.A., Olesen, O. 2002: Magnetic susceptibility of Mesozoic and Cenozoic sediments off Mid Norway and the role of siderite: implications for interpretation of high-resolution aeromagnetic anomalies. *Mar. and Petr. Geology* 19, 1115-1126.
- Naudy, H. 1971: Automatic determination of depth on aeromagnetic profiles. *Geophysics* 36, No. 5, pp. 717-722.
- Nordgulen, Ø., Braathen, A., Corfu, F., Osmundsen, P.T. & Husmo, T. 2002: Polyphase kinematics and geochronology of the late-Caledonian Kollstraumen detachment, north-central Norway. *Norsk Geologisk Tidsskrift* 82, 299-316.
- Norges geologiske undersøkelse 1992: Aeromagnetisk anomalikart, Norge M 1:1 mill, Norges geologiske undersøkelse.
- Olesen, O. & Myklebust, R. 1989: LAS-89, Lofoten Aeromagnetic Survey 1989,

- Interpretation report. *NGU Report 89.168*, 54 pp.
- Olesen, O., Henkel, H., Kaada, K. & Tveten, E. 1991: Petrophysical properties of a prograde amphibolite - granulite facies transition zone at Sigerfjord, Vesterålen, Northern Norway. In: P. Wasilewski & P. Hood (Eds.). *Magnetic anomalies — land and sea. Tectonophysics 192*, 33-39.
- Olesen, O. & Torsvik, T.H. 1993: Interpretation of aeromagnetic and gravimetric data from the Lofoten-Lopphavet area. *NGU Report 93.032*, 77 pp.
- Olesen, O. & Skilbrei, J.R. 1993: Magnetic interpretations In: Løseth, H., Gading, M., Hansen, O., Leith, L., Mukhopadhyay, M., Myhr, M.B., Olesen, O., Ritter, U., Skilbrei, J.R. & Sylta, Ø. 1993: Vøring Basin analysis. *IKU Report 23.2439.00/01/93*.
- Olesen, O., Torsvik, T.H., Tveten, E. & Zwaan, K.B. 1993: The Lofoten - Lopphavet Project, an integrated approach to the study of a passive continental margin, Summary report. *NGU Report 93.129*, 54 pp.
- Olesen, O. & Smethurst, M.A. 1995: NAS-94 Interpretation Report, Part III: Combined interpretation of aeromagnetic and gravity data. *NGU Report 95.040*, 50 pp.
- Olesen, O., Gellein J., Håbrekke H., Kihle O., Skilbrei J. R., & Smethurst M. 1997a: *Magnetic anomaly map Norway and adjacent ocean areas, scale 1:3 million*. Norges geologiske undersøkelse, Trondheim, Norway.
- Olesen, O., Torsvik, T.H., Tveten, E., Zwaan, K.B., Løseth H. & Henningsen, T. 1997b: Basement structure of the continental margin in the Lofoten-Lopphavet area, northern Norway: constraints from potential field data, on-land structural mapping and palaeomagnetic data. *Nor. Geol. Tidsskr. 77*, 15-33.
- Olesen, O., Lundin, E., Nordgulen, Ø., Osmundsen, P.T., Skilbrei, J.R., Smethurst, M.A., Solli, A., Bugge, T. and Fichler, C., 2002. Bridging the gap between the onshore and offshore geology in Nordland, northern Norway. *Norwegian Journal of Geology*, 82, 243-262.
- Osmundsen, P.T., Braathen, A., Nordgulen, Ø., Roberts, D., Meyer, G.B. & Eide, E. 2003: The Devonian Nesna shear zone and adjacent gneiss-cored culminations, North-central Norwegian Caledonides. *Journal Geol. Soc. London 160*, 1-14.
- Phillips, J.D. 1979: ADEPT: A program to estimate depth to magnetic basement from sampled magnetic profiles. *U.S. geol. Surv. open-file report 79-367*, 35 pp.
- Planke, S., Skogseid, J. & Eldholm, O. 1991: Crustal structure off Norway, 62° to 70° north. *Tectonophysics 189*, 91-107.
- Reid, A.B., Allsop, J.M., Granser, H., Millett, A.J., Sommerton, I.W., 1990. Magnetic interpretation in three dimensions using Euler deconvolution, *Geophysics 55*, 80-91.
- Roeser, H.A. 1993: Magnetische Messungen auf See. *Deutsche Geoph. Gesellschaft Mittlg. 2*, 11-24.
- Rykkelid, E. & Andresen, A. 1994: Late Caledonian extension in the Ofoten area, northern Norway. *Tectonophysics 231*, 157-169.
- Saunders, A.D., Fitton, J.G., Kerr, A.C., Norry, M.J. & Kent, R.W. 1997: The North Atlantic Igneous Province. In: Mahoney, J.J. & Coffin, M.L. (eds). *Large Igneous Provinces*, Geophysical Monograph Series, American Geophysical Union, Washington, DC, 45-93.

- Schlenger, C. M. 1985: Magnetization of lower crust and interpretation of regional magnetic anomalies: Example from Lofoten and Vesterålen, Norway. *J. Geophys. Res.* 90, 11484-11504.
- Schmidt, S. and Götze, H.-J., 1998: Interactive visualization and modification of 3D models using GIS functions. *Phys. Chem. Earth*, 23(3): 289-296.
- Osmundsen, P.T., Braathen, A., Roberts, D. & Gjelle, S. 2000: Late- to Post-Caledonian tectonics in Mid Norway: The Nesna shear zone and its regional implications. Abstract 24<sup>th</sup> Nordic Geological Winter Meeting, Trondheim. p. 133.
- Reid, A.B., Allsop, J.M., Granser, H., Millett, A.J. & Sommerton, I.W. 1990: Magnetic interpretation in three dimensions using Euler deconvolution. *Geophysics* 55, 80-91.
- Schönharting, G. & Abrahamsen, N. 1989: Paleomagnetism of the volcanic sequence in hole 642E, ODP leg 104, Vøring Plateau, and correlation with early Tertiary basalts in the North Atlantic. *In* Eldholm, Thiede, Taylor *et al.* (Eds.) *Proceedings of the Ocean Drilling Program, Scientific Result 104*, College Station, TX, 911-920.
- Sellevoll, M.A. 1983: A study of the Earth in the island area of Lofoten- Vesterålen, northern Norway. *Nor. geol. unders.* 380, 235-243.
- Sellevoll, M.A., Olafsson, I., Mokhtari, M., Gidskehaug, A. 1988: Lofoten margin, North Norway: crustal structure adjacent to the ocean-continent transition. *Nor. geol. unders. Special Publ.* 3, 39-48.
- Simpson, R.W., Jachens, R.C., & Blakely, R.J. 1983: AIRYROOT: A Fortran program for calculating the gravitational attraction of an Airy isostatic root out to 166.7 km. *United States Department of the Interior, Geological Survey, Open-File Report 83-883*, 24 pp.
- Sinton, C.W., Hitchen, K. & Duncan, R.A. 1998: Ar<sup>40</sup>-Ar<sup>39</sup> geochronology of silicic and basic volcanic rocks on the margins of the North Atlantic. *Geol. Mag.*, **135**, 161-170.
- Skilbrei, J.R., Kihle, O., Olesen, O., Gellein, J., Sindre, A., Solheim, D. & Nyland, B. 2000: Gravity anomaly map Norway and adjacent ocean areas, scale 1:3 Million. Geological Survey of Norway, Trondheim.
- Skilbrei, J.R. & Kihle, O. 1999: Display of residual profiles versus gridded image data in aeromagnetic study of sedimentary basins: A case history. *Geophysics* 64, 1740-1747.
- Skilbrei, J.R., Olesen, O., Osmundsen, P.T., Kihle, O., Aaro, S. and Fjellanger, E., 2002. A study of basement structures and onshore-offshore correlations in Central Norway. *Norsk Geologisk Tidsskrift* 82, 263-279.
- Skogseid, J., Pedersen, T., and Larsen, V.B., 1992: Vøring Basin: subsidence and tectonic evolution. *In* Larsen, R.M., Brekke, H. Larsen, B.T. & Talleraas, E. (Eds.) *Structural and Tectonic Modelling and its Application to Petroleum Geology. NPF Special Publication, Elsevier, Amsterdam*, 55-82.
- Smith, W. H. F. & Sandwell, D. T. 1997: Global sea floor topography from satellite altimetry and ship depth soundings. *Science* 277, 1956-1962.
- Stoker, M.S., Hitchen, K. & Graham, C.C. 1993: Geology of the Hebrides and West Shetland shelves, and adjacent deep-water areas. *United Kingdom offshore*

- regional report, British Geological Survey. 149 pp.*
- Svela, P.T. 1971: Gravimetriske undersøkelser av Lofoten-Vesterålen området. *Unpubl. Cand. real. thesis, Univ. of Bergen*, 131 pp.
- Talwani, Udintsev *et al.* (Eds.) 1978: Initial reports of the Deep Sea Drilling Project, Supplements to Vol. 38, 39, 40 and 41. *Govt. Printing Office, Washington, D.C.*
- Thompson, D.T., 1982. EULDPH: A new technique for making computer-assisted depth estimates from magnetic data. *Geophysics* 47, 31-37.
- Torsvik, T.H. & Olesen, O. 1992: PDEPTH - calculation of depth to magnetic basement from profile data. *Unpublished NGU Report 92.212*, 26 pp.
- Torsvik, T.H. & Fichler, C. 1993: GDEPTH - gravity inversion and calculation of basement depths. *Unpublished NGU Report 93.066*, 33 pp.
- Tsikalas, F., Faleide, J.I. & Eldholm, O. 2001: Lateral variations in tectono-magmatic style along the Lofoten-Vesterålen volcanic margin off Norway. *Marine and Petroleum Geology* 18, 807-832.
- Tsikalas, F., Eldholm, O. & Faleide, J.I. 2002: Early Eocene sea floor spreading and continent-ocean boundary between Gleipne and Senja fracture zones in Norwegian-Greenland Sea. *Marine Geophysical Researches* 23, 247-270.
- Underhill, J.R., Sawyer, M.J., Hodgson, P., Shallcross, M.D. & Gawthope, R.L. 1997. Implications of fault scarp degradation for the Brent Group prospectivity, Ninian Field, Northern North Sea. *American Association of Petroleum Geologists Bulletin*, 81, 999-1022.
- Verhoef, J., Roest, W.R., Macnab, R., Arkani-Hamed, J. & Members of the Project Team 1996: Magnetic anomalies of the Arctic and North Atlantic Oceans and adjacent land areas. *GSC Open File 3125, Parts a and b* (CD-ROM and project report), Geological Survey of Canada, Dartmouth NS.
- Vogt, P.R., Bernero, C., Kovacs, L.C. & Taylor, P. 1981: Structure and plate tectonic evolution of the marine Arctic as revealed by aeromagnetism. *Oceanol. Acta No. SP*, 25-40.
- Zwaan, K.B. 1995: Geology of the West Troms Basement Complex, northern Norway, with emphasis on the Senja Shear Belt: a preliminary account. *Norges geologiske undersøkelse Bull.* 427, 33-36.
- Åm, K. 1975: Aeromagnetic basement complex mapping north of latitude 62°N, Norway. *Nor. geol. unders.* 316, 351-374.



## List of figures and tables

### Figures

Figure 1.1 Bathymetry and topography, Nordland area, 100 and 500 m contour intervals

Figure 2.1 Compilation of aeromagnetic surveys in the Nordland area. NRL-73 US Naval Research Laboratory 1973, RAS-03 - Røst Aeromagnetic Survey 2003, SPT-93 - Simon Petroleum Technology 1993, LAS-89 - Lofoten Aeromagnetic Survey 1989, NAS-94 - Nordland Aeromagnetic Survey 1994, VAS-1998 - Vestfjorden Aeromagnetic Survey 1998. The latter four surveys were acquired by the Geological Survey of Norway.

Figure 2.2 Compilation of gravity surveys in the Nordland area. KMS – Kort og Matrikelstyrelsen, Denmark, NPD/SK- Norwegian Petroleum Directorate/ Norwegian Mapping Authority.

Figure 2.3 Locations of petrophysical samples on the mainland and offshore Nordland shown as blue circles (Olesen et al. 1997b, 2002, Mørk & Olesen 1995, Mørk et al. 2002).

Figure 3.1 Aeromagnetic anomaly map, Nordland area

Figure 3.2 Aeromagnetic anomaly map, 25 km high-pass filtered, Nordland area

Figure 3.3 Free-air gravity map, Nordland area

Figure 3.4 Bouguer gravity map, Nordland area

Figure 3.5 Isostatic residual, Bouguer gravity map, Nordland area

Figure 3.6 Bouguer gravity, 100 km high-pass filtered, Nordland area

Figure 3.7 Geophysical interpretation map, Nordland area

Figure 4.1 Sketch map of the main structural elements in the Norwegian-Greenland Sea area before opening of the Atlantic (Modified from Hartz et al. 2002, Braathen et al. 2002, Olesen et al. 2002 and Skilbrei et al. 2002). The bold black lines show the late Caledonian detachment zones.

Figure 4.2 Main structural elements in the Nordland area (Blystad et al. 1995)

Figure 4.3 Magnetic lineations and structural elements off Norway (Tsikalas et al. 2002). LS, VS, AS, Lofoten, Vesterålen, and Andøya margin segments, respectively; SAZ, Surt accommodation zone; NH, UH, RH, JH, Nyk, Utgard, Røst, and Jennegga highs, respectively; LR, UR, Lofoten and Utrøst ridges, respectively; HB, Havbåen sub-basin. 23-R and COB-R are conjugate features rotated from the Greenland margin.

Figure 5.1. Depth to Moho compiled from refraction seismic studies (Lund 1979, Kinck et al. 1993, Mjelde et al. 1992, 1993, 1997, 1998, Sellevoll 1983) and gravity interpretations (Olesen et al. 1997, 2002). The black lines show the interpreted profiles within the present 3D model. Blue lines show the refraction seismic lines. The pale blue line denotes the interpreted continent-ocean boundary.

Figure 5.2 3D perspective map of the basement in Nordland area (seen from the south).

Figure 5.3 3D perspective map of the magnetic basement in Nordland area showing that there is a substantial amount of low-magnetic basement rocks below the deepest part of the Vestfjorden, Træna and Ribban basins in addition to the Nordland Ridge (view

from the southwest).

Figure 5.4 Profile 14 of the 3D model. The upper panel shows the gravity anomaly (offshore: Free-Air anomaly, onshore: Bouguer anomaly), the middle panel the magnetic anomaly and the lower panel the modelled density/magnetic cross-section. Black numbers are density values in  $\text{gr/cm}^3$ , white numbers represent magnetic susceptibilities. The black-white dotted line indicates the Curie depth. See Figs 3.1 - 3.6 and Maps 1 - 7 for exact location of the profile and text for further details.

Figure 5.5 Profile 15 of the 3D model. See description of Fig. 5.4 for further details.

Figure 5.6 Profile 16 of the 3D model. See description of Fig. 5.4 for further details.

Figure 5.7 Profile 17 of the 3D model. The location of the profile is close to the assumed location of the Bivrost Transfer Zone. The Myken Volcanic Complex in the central part of the profile is causing a prominent gravity anomaly. See description of Fig. 5.4 for further details.

Figure 5.8 Profile 18 of the 3D model. The profile is the first immediately to the north of the Bivrost Lineament. See description of Fig. 5.4 for further details.

Figure 5.9 Profile 19 of the 3D model. The location of the line is coinciding with the OBS line 2 (Mjelde et al. 1992). See description of Fig. 5.4 for further details.

Figure 5.10 Profile 20 of the 3D model. The location of the line is coinciding with OBS Lines 1 and 3 (Mjelde et al. 1992). See description of Fig. 5.4 for further details.

Figure 5.11 Profile 21 of the 3D model. The location of the line is coinciding with OBS Line 4 (Mjelde et al. 1992). See description of Fig. 5.4 for further details.

Figure 5.12 Profile 22 of the 3D model. The location of the line is coinciding with OBS line 5 (Mjelde et al. 1992). See description of Fig. 5.4 for further details.

Figure 5.13 Profile 24 of the 3D model. On this profile the magnetic signature over the Lofoten Ridge has a maximum of 1500 nT. See description of Fig. 5.4 for further details.

Figure 5.14 Regional basement faults within Nordland area. GF - Grønna fault, HF - Hamarøya fault, NSZ - Nesna shear zone, SSZ - Sagfjord shear zone; FH - Flakstad High; JH - Jennegga High; SH - Sandflesa High; RH - Røst High; NH - Nyk High; RoH - Rødøy High; GH - Grønøy High; VFZ - Vesterdjupet Fault Zone; BSFC - Bothnian-Senja fault complex; VVF - Vestfjorden-Vanna fault complex; WLBF - Western Lofoten border fault; ELBF - Eastern Lofoten border fault; MC - Myken volcanic complex. The nomenclature is adapted from Andresen & Forslund (1987), Blystad et al. (1995), Løseth & Tveten (1996), Olesen et al. (1997b), Tsikalas et al. (2001) and Braathen et al. (2002).

Figure 5.15 Regional basement structures within the Nordland area. The depth to basement surface represents depth to crystalline rocks. NSZ - Nesna shear zone, SSZ - Sagfjord shear zone; GF - Grønna fault, HF - Hamarøya fault; FH - Flakstad High; JH - Jennegga High; SH - Sandflesa High; RH - Røst High; NH - Nyk High; RoH - Rødøy High; GH - Grønøy High; VFZ - Vesterdjupet Fault Zone; BSFC - Bothnian-Senja fault complex; VVF - Vestfjorden-Vanna fault complex; WLBF - Western Lofoten

border fault; ELBF - Eastern Lofoten border fault; MC - Myken volcanic complex. The nomenclature is adapted from Andresen & Forslund (1987), Blystad et al. (1995), Løseth & Tveten (1996), Olesen et al. (1997b,) Tsikalas et al. (2001) and Braathen et al. (2002).

Figure 5.16 Shaded relief version of magnetic data of the Utgard High and surrounding areas, together with stacked magnetic profiles. Line numbers are shown. Rectangles represent location of Naudy depth-solutions. See text for explanation, and next figure. Note that coordinates are in UTM zone 33.

Figure 5.17 Example of Naudy depth solution along line 80, crossing the Utgard High. Numbers inside the rectangle refer to depth to the top (upper number), Susceptibility (S), and thickness of block (T), representing the basement block of the Utgard High. Similar depth solutions were obtained also from other lines crossing the Utgard High. The solutions have been plotted on the maps, together with Euler- and autocorrelation-estimates (Figs. 3.1- 3.7, Maps 1-6).

Figure 5.18 Magnetic forward model along line 44. The model shows that the main anomaly above the Utgard High can be caused by the basement block. The rather sharp negative anomaly on the western side of the high (eastern part of the Någrind Syncline) is explained by remanent magnetisation of dolerite intrusions that occur at a depth of around 5000 m in the syncline. Applied magnetic susceptibility of the basement is 0.01 (blue 'basement body'), 0.0027 (brown basement body), and 0.01 (brown basement body, left in profile). The dolerite has a negative susceptibility of  $-0.027$  (units in SI).

Figure 5.19 Alternative forward model along line 44, without dolerite intrusion in the Någrind Syncline. Compare with Fig. 5.18. Note that a poorer fit between observed and modelled magnetic curve is achieved See text for explanation.

## Tables

Table 2.1. Offshore aeromagnetic surveys compiled for the present study (Figs. 3.1 & 3.2, Maps 1 & 2). We included 27.000 km of the NAS-94 survey. The RAS-03 survey included 2.300 km refling of the LAS-89 survey.

Table 2.2. On land aeromagnetic surveys compiled for the present interpretation (Figs. 3.3 - 3.6).

Table 2.3. Gravity surveys on land (Skilbrei et al. 2000) included in the present study (Fig. 2.2).

Table 2.4. Arithmetical mean and standard deviation of density, susceptibility and Q-values measured on 4700 hand specimens from the Nordland area. The measurements were extracted from the national petrophysical database at the Geological Survey of Norway. Olesen et al. (1991), Mørk & Olesen (1995) and Olesen et al. (1997b,2002) have reported more detailed presentations of the statistical data. SI units are used.

Table 2.5. Density (in  $1000 \cdot \text{kg/m}^3$ ) of sedimentary sequences from density logs of wells in the Nordland area and refraction seismic studies. (2.78\*) = average density of 639 rock samples from the Precambrian on the Lofoten and Vesterålen archipelago (Olesen et al. 1997b, 2002).

Table 2.6. Magnetic properties of igneous rocks from drilling in the Vøring area within the Deep Sea Drilling Project (DSDP) and Ocean Drilling Program (ODP) in 1974 and 1985, respectively (<sup>1</sup>Kent & Opdyke 1978, <sup>2</sup>Eldholm et al. 1987). The ODP susceptibility data are claimed to be cgs-units, but they are most likely in SI-units, because a corresponding magnetite content of 30-40 % in the volcanics is highly unlikely. A log diagram of the 642E well in Schönharting & Abrahamsen (1989) supports this conclusion.

## Maps

Map 1 Aeromagnetic anomaly map, Nordland area, Scale 1:500.000

Map 2 Aeromagnetic anomaly map, 25 km high-pass filtered, Nordland area, Scale 1:500.000

Map 3 Free-air gravity map, Nordland area, Scale 1:500.000

Map 4 Bouguer gravity map, Nordland area, Scale 1:500.000

Map 5 Isostatic residual, Bouguer gravity map, Nordland area, Scale 1:500.000

Map 6 Bouguer gravity, 100 km high-pass filtered, Nordland area, Scale 1:500.000

Map 7 Geophysical interpretation map, Nordland area, Scale 1:500.000